Policy Research Working Paper 10760

Droughts Worsen Air Quality by Shifting Power Generation in Latin America and the Caribbean

Mathilda Eriksson
Alejandro del Valle
Alejandro de la Fuente

WORLD BANK GROUP
Poverty and Equity Global Practice
May 2024

Policy Research Working Paper 10760

Abstract

This paper studies how air quality around combustion power plants changes in response to hydrological droughts that affect hydropower generation. Using fixed-effect and post-double selection methods, the paper analyzes a unique plant-level panel of fine particulate matter concentrations and meteorological conditions spanning 20 years at monthly frequency. The findings show that, on average, hydrological droughts lead to 0.83 micrograms per cubic meter excess fine particulate matter, equivalent to a 5.3 percent increase from non-drought conditions. Counterfactual simulations for the region indicate that this excess fine particulate matter may have resulted in up to 10,000 premature deaths annually. Combining the estimates with climate, demographic, and policy projections, the paper also shows that this health burden will likely persist over the next four decades.

This paper is a product of the Poverty and Equity Global Practice. It is part of a larger effort by the World Bank to provide open access to its research and make a contribution to development policy discussions around the world. Policy Research Working Papers are also posted on the Web at http://www.worldbank.org/prwp. The authors may be contacted at meriksson@gsu.edu or adelafuente@worldbank.org.

Droughts Worsen Air Quality by Shifting Power Generation in Latin America and the Caribbean

Mathilda Eriksson,* Alejandro del Valle,*
and Alejandro de la Fuente†

JEL Classifications: I1, I3, Q4, Q5, Q53, Q54
Keywords: Drought, Electricity Generation, Air Quality, Health, Poverty, Climate Change

*Georgia State University, Maurice R. Greenberg School of Risk Sciences, Atlanta, GA.
†World Bank, Poverty, and Equity Global Practice, Washington, D.C.
Correspondence: meriksson@gsu.edu

This is a background paper for the Regional Study on Climate and Poverty in Latin America and the Caribbean supported by the Climate Support facility Whole-of-Economy Program, administered by the World Bank. We want to thank Laura Bakkensen, Judson Boomhower, Dylan Brewer, Olivier Deschenes, Xavier Gine, Matthew Kahn, Namrata Kala, Vikalp Mishra, Seyhun Sakalli, Casey Wichman, Esha Zaveri, and Eric Zou, as well as seminar and conference participants at Georgia State University, Imperial College London, Georgia Institute of Technology, Javeriana University, OECD, and the World Bank for helpful comments.

1 Introduction

Electricity generation is a water-intensive process, with most power plants requiring water to spin hydroelectric turbines or cool thermoelectric generators (Sanders, 2015). In Latin America and the Caribbean (LAC), approximately half of the total power generation comes from hydropower, while the other half comes from combustion power, including coal, oil, gas, and biomass (IEA, 2021). Because hydrological droughts predominantly limit the generation capacity of hydropower plants, droughts can shift generation to combustion power plants. A plausibly important but understudied consequence of this shift in generation is the worsening of local air quality. Changes in air quality are a first-order concern, as exposure to fine particle air pollution ($PM_{2.5}, < 2.5$ μm) is detrimental to human health (Dockery et al., 1993; Pope III et al., 2002, 2009; Cohen et al., 2017), with recent studies showing that even low levels of exposure lead to adverse health outcomes (Weichenthal et al., 2022). With nearly half a billion individuals in LAC residing near a combustion power plant and climate change leading to more frequent and severe hydrological droughts in the region, a key question is determining how air quality changes in response to this shift in electricity generation.

In this paper, we fill this gap by quantifying the relationship between hydrological droughts and increased $PM_{2.5}$ concentrations around combustion power plants in LAC. We begin by assembling a monthly frequency power plant-level panel covering the 2000 to 2020 period. The panel provides information on both $PM_{2.5}$ concentrations in the proximity of combustion power plants and market-level measures of the level of hydropower generation capacity in water stress. These market-level measures are derived from granular watershed-level measures of hydrological drought. Our preferred market-level measure is the fraction of hydropower generation capacity affected by drought (FHD). The panel also provides information on an extensive set of meteorological factors, emissions from wildfires, proxies of electricity demand, and characteristics of power plants. Using this dataset and fixed effect methods, we estimate the excess air pollution created by changes in the FHD. Our estimates have a causal interpretation because, conditional on meteorological factors, changes in electricity demand, and seasonal trends, hydrological droughts create a plausibly exogenous shock to hydropower generation. Because hydrological droughts can increase $PM_{2.5}$ through alternative mechanisms, such as increasing the likelihood of wildfires, we exclude plant-month observations affected by wildfires.

Our results fall into four categories. The first set of results shows that hydrological

droughts considerably increase $PM_{2.5}$ concentrations around combustion power plants. At average FHD levels, we find an increase of 0.83 $\mu g/m^3$, which increases $PM_{2.5}$ concentrations from 15.76 in the absence of hydrological droughts to 16.59 $\mu g/m^3$ (i.e., roughly a 5.3 percent increase). With World Health Organization guidelines categorizing $PM_{2.5}$ concentration greater than 5 $\mu g/m^3$ as harmful to human health (WHO, 2021), the excess $PM_{2.5}$ created by hydrological droughts will likely lead to a considerable health burden for the region.

The second set of results highlights that the most likely mechanism for the documented increase in $PM_{2.5}$ is the shift in electricity generation from hydropower to combustion power plants. Specifically, we show a clear dose-response gradient with $PM_{2.5}$ monotonically increasing with FHD. We also provide evidence from two placebo exercises that rule out wildfires and dust storms as plausible drivers of our results. Specifically, we test and fail to find evidence of FHD increasing $PM_{2.5}$ around clean power plants (solar, wind, and nuclear) or around combustion power plants in the years before they become operational. We also rule out changes in electricity demand or other meteorological factors driving the results by controlling for these factors in our specification. In our main specification, we assume that these effects are additive and linear. Still, our result holds even after relaxing these assumptions and using the post-double selection method of Belloni et al. (2014) to test far more flexible specifications. The pattern of heterogeneous effects with respect to plant size and fuel type further bolsters the case for the shift in generation to combustion power plants as the primary mechanism. Specifically, we find that the effects on excess $PM_{2.5}$ are largest for smaller power plants and those that use oil or biomass and more muted among larger power plants and those that use coal. These results are consistent with the idea that smaller power plants are more able to respond during a drought as they tend to be air-cooled, while larger power plants tend to be water-cooled. Another possible reason the effect is more muted among larger power plants (mainly coal) is their limited flexibility (i.e., they provide baseload generation).

The third set of results quantifies the number of lives lost building on our estimates of drought-induced excess $PM_{2.5}$, demographic data on the population exposed, and well-established concentration-response functions from the literature that documents the adverse health effects of $PM_{2.5}$ (e.g., Deryugina et al. (2019); Liu et al. (2019)). Our preferred counterfactual calculation shows that the region experiences as many as 10,000 premature deaths per year. The monetized losses from the lives lost using conservative estimates of the value of a statistical life indicate an associated cost in the order of $12 billion (constant 2019 USD) per year.

We also characterize the population residing in close proximity to combustion power plants and show that the burden of excess $PM_{2.5}$ falls disproportionately among groups with lower socioeconomic status.

The fourth set of results projects these costs into the future, accounting for possible changes in the climate, demography, and the electricity sector. Specifically, we extend the counterfactual calculations until 2059, which roughly corresponds to the expected operational lifespan of the combustion power plants in service. We begin by computing the evolution of the FHD using data from 22 climate and earth system models under three Shared Socioeconomic Pathways (SSPs). Concerningly, for the region, we find that the FHD is expected to increase between 22 and 24 percent over the next four decades. Consistent with the increase in the FHD, we also find that premature deaths and monetized losses are also likely to increase. When assessing the effect of the SSPs in conjunction with three highly stylized electricity sector scenarios, we find that merely flattening out the losses would require the most optimistic SSP scenario in conjunction with an electricity sector scenario where combustion power plants are phased out following regional pledges. These results are important because they indicate that the health burden of excess $PM_{2.5}$ is largely permanent over the next four decades and is a first-order concern for policy makers in the region. Another important feature of these results is that there are considerable differences in sub-regional trends, for example, with the Andean Region (Colombia, Ecuador, and Peru) poised to experience a decrease in hydrological droughts and consequently in their FHD.

Our paper contributes to several stands of literature. Most narrowly, it extends recent work in the U.S. quantifying the relationship between hydrological droughts, energy generation, and air quality (Eyer and Wichman, 2018; Herrera-Estrada et al., 2018; Qiu et al., 2023). Specifically, we demonstrate that this relationship also exists in LAC, we recover the first region-wide estimates of excess $PM_{2.5}$ for the region, and we offer three novel insights about this relationship. First, we provide the first estimates of the nexus between hydrological droughts and excess $PM_{2.5}$ created by combustion power plants that use oil and biomass. We also show that these plants lead to some of the largest decreases in air quality. These findings are important because oil and biomass power plants are common in developing countries. Second, we show that the link between hydrological droughts and worsening air quality can be observed even for short-duration droughts. We can document this response because we observe small hydropower plants (greater than 1 MW), which often lack dams, and as a result, their generation capacity is more immediately affected by droughts. Third, we show that small-capacity com-

bustion power plants, common in the region and more likely to be air-cooled and less affected by droughts, lead to considerable increases in excess $PM_{2.5}$. Overall, our findings complement the U.S. literature by highlighting that the threat to air quality posed by hydrological droughts is more significant for developing economies.

More broadly, our paper speaks to the literature that aims to quantify the economic damage of climate change (see Auffhammer, 2018, and references therein) by providing region-wide estimates for LAC of the societal cost that hydrological droughts impose by altering electricity generation, and by projecting these losses under several climate change scenarios. We also contribute to the literature on environmental inequalities (see Banzhaf et al., 2019, and references therein) by documenting that excess $PM_{2.5}$ falls disproportionately among those with lower socioeconomic status. We thereby highlight a novel channel through which droughts reinforce socioeconomic inequalities.

The paper is organized as follows. Section 2 describes the data. Section 3 presents the identification strategy and the results. Section 4 provides counterfactual calculations of the losses created by excess $PM_{2.5}$. Section 5 presents projections of losses based on our results and climate models. Section 6 presents robustness checks. Section 7 concludes.

2 Description of the data

We construct a power plant-level panel dataset to study whether hydrological droughts impact $PM_{2.5}$ concentrations by shifting electricity production towards combustion power plants. This unique dataset combines market-level measures of the level of distress by hydropower plants, derived from a granular watershed-level measure of hydrological drought, with information on $PM_{2.5}$ concentrations within 50 km of each power plant. This monthly dataset covers all Latin American and Caribbean countries between 2000 and 2020.

The starting point for our panel dataset is the Global Power Plant Database detailed in Byers et al. (2018).[1] This database provides detailed information on the geolocation, capacity, fuel type, and commissioning year for all power plants with generators above 1 megawatt (MW). This feature of our dataset is important because little is known about the pollution burden created by plants with smaller

[1] https://datasets.wri.org/dataset/globalpowerplantdatabase, Dataset Last Updated June 2, 2021.

capacities. In our sample, 67 percent of plants have a capacity lower than 30 MW.[2]

Next, we augment this dataset with market-level measures of the degree of hydrological drought faced by hydropower plants at monthly frequency during the 2000 to 2020 period. The process of computing these measures of drought involves several steps. In the first step, we follow existing literature and use runoff anomalies to measure hydrological drought (Herrera-Estrada et al., 2018; IEA, 2021; Qiu et al., 2023). Runoff is the depth of water accumulated over time in the soil and is a valuable indicator of drought or flood conditions. Runoff anomalies indicate a period where water availability is above or below normal. Specifically, we define runoff anomalies as the difference between the monthly runoff and its corresponding average value over the reference period (2000 to 2019). To measure runoff anomalies, we use data from the International Energy Agency Weather for Energy Tracker database[3] (IEA and CMCC, 2022). This database provides information derived from the ERA 5 reanalysis on monthly total runoff anomalies (surface and subsurface) measured in millimeters per hour (mm/h) at a spatial resolution of 0.25°x0.25°.

In the second step, we determine the watershed of each hydropower plant in the sample. The watershed is the area over which water would accumulate for use by the hydropower plant. To compute these areas, we use the hydro basin polygons (areas where water collects and may flow) from the HydroSHEDS database[4] (Lehner and Grill, 2013). This dataset is produced from digital elevation maps and hydrological models. Next, following standard engineering practices for each hydropower plant, we delineate the watershed by tracing all of the upstream basins (Pfastetter level 12) that flow in the direction of the power plant. The resulting dataset provides a watershed for each hydropower plant.

In the third step, we overlay the information on runoff anomalies with the watershed delineations and compute the average monthly runoff anomalies for each watershed. Figure A1 in the appendix plots the evolution of runoff anomalies for the region in panel A and for sub-regions defined by the IEA in panel B. The figures reveal considerable sub-regional heterogeneity even during periods of significant overall drought, such as 2015 to 2020.

[2]Power plants with a capacity exceeding 30 MW are usually categorized as large plants by the US Department of Energy.

[3]https://www.iea.org/data-and-statistics/data-tools/weather-for-energy-tracker

[4]https://www.hydrosheds.org/products/hydrobasins

To measure the impact of anomalies with a duration greater than one month, we repeat the previous calculation using a moving average of the runoff anomalies over the past three, six, nine, and 12 months. The resulting dataset provides detailed information on whether water availability conditions are above or below normal for each hydropower plant. Figure 1 shows the distribution of the hydropower plants in our sample and provides a visual example of how the hydrological drought dataset is constructed.

Figure 1: Hydropower plants, watersheds, and runoff anomalies

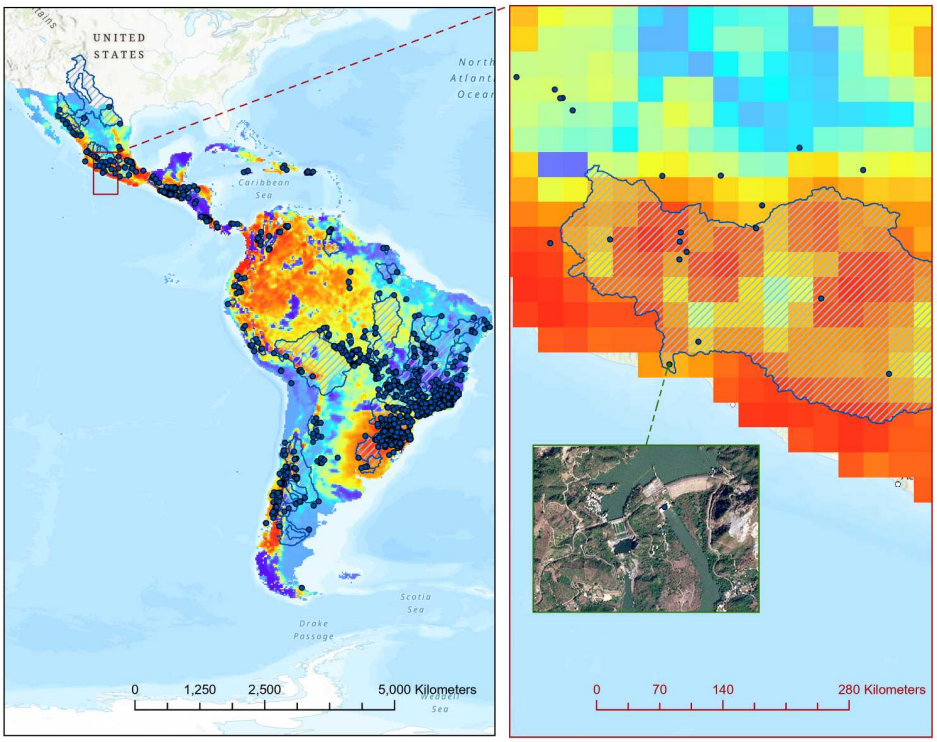

Notes: Dots represent hydropower plants (N = 1,069), hatched areas show hydropower watersheds, and the color gradient indicates the average monthly runoff anomalies ranging from low (red) to high (blue). The right panel zooms into the hydropower plant Infernillo in Mexico (October 2020) and shows its watershed.

In the fourth step, we use the information derived in the previous step to compute market-level measures of the hydropower generation affected by hydrological drought. In the absence of systematic information on the boundaries of electri-

cal markets within countries, we define each electricity market using the country boundaries. As documented by Timilsina et al. (2021), there is little cross-border trade in the region, with less than 5 percent of total regional generation being transmitted across countries.

Our preferred market-level measure is the fraction of hydropower generation capacity affected by drought (FHD). To construct this measure, we create a binary variable equal to one when the watershed of a hydropower plant has less water available than normal in the past three months (mean negative runoff anomaly) and zero otherwise. Next, we compute the average of this variable for each market and month. To account for the greater impact that larger plants experiencing drought can have on electricity generation, we weigh this average by plant capacity. We define droughts over a relatively short period (three months) because small hydropower plants are common in the region, and for these plants, even short-run changes in water availability may imply reduced generation capacity. Nonetheless, to check whether our results are robust to alternative definitions of drought duration, we also compute the FHD variable using the moving average of runoff anomalies in the past one, six, nine, and 12 months.

We also acknowledge that different aggregation methods prioritize different features of the data. With our primary approach, we exploit the spatial granularity of our data and aim to capture the effect of both local and regional droughts by identifying periods in which hydropower generation declines due to water availability being below normal levels. However, to ensure that we study the full scope of our data, we also compute our market-level measure in other ways. For instance, we prioritize the number of plants affected in an alternative computation using an arithmetic average instead of a capacity-weighted average.

Additionally, we calculate market-level measures considering only the most severe droughts. To operationalize this alternative definition, we follow Herrera-Estrada et al. (2018) and create a binary variable that equals one only when runoff anomalies are one standard deviation below normal levels. We then compute the average of the variable for each market and month. These and other variations of the market-level measures help us understand the effects of extreme drought. We also compute a measure that directly gauges the intensity of the drought by calculating the average runoff anomaly for each market and month. One downside of this measure is that, in the case of non-market-wide droughts, it may incorrectly assume that negative anomalies experienced by some hydropower plants can be offset by positive anomalies experienced by other plants.

With our battery of market-level measures added to the panel using country and month-year identifiers, we focus on measuring the concentration of $PM_{2.5}$ around combustion power plants. Specifically, we use information on monthly mean surface $PM_{2.5}$ concentrations measured in micrograms per cubic meter ($\mu g/m^3$) from the V5.GL.03 dataset detailed in Van Donkelaar et al. (2021).[5] This geophysical-hybrid dataset provides estimates of $PM_{2.5}$ concentrations by combining data from satellites, chemical transport models, and ground-based monitors. It provides information at 0.01°x0.01° resolution at a monthly frequency between 1998 and 2021. Because previous literature has shown that there are considerable health effects within 50 km of a power plant (Qiu et al., 2023; Fraenkel et al., 2024; Clay et al., 2016), we compute the average $PM_{2.5}$ concentrations for every plant and month at this distance and at 10 km. Figure 2 shows the distribution of the combustion plants in our sample and provides a visual example of how the $PM_{2.5}$ concentrations are calculated. To run placebo exercises, we also compute these measures of $PM_{2.5}$ concentrations within 50 km of non-combustion power plants (i.e., solar, wind, nuclear, geothermal).

Next, we include in the dataset variables that can help us account for factors that confound the relationship between $PM_{2.5}$ concentrations and our market-level measures of drought. Wildfires, which are more prevalent during droughts and lead to higher $PM_{2.5}$ concentrations (McClure and Jaffe, 2018), are a particular source of concern. To limit the influence of surface $PM_{2.5}$ related to wildfires, we follow Qiu et al. (2023) and omit observations plausibly affected by wildfires. Specifically, we use data from the Global Fire Emissions Database version 4 (GFED4s)[6] described in Van Der Werf et al. (2017). This dataset provides monthly information on carbon emissions from fires at a spatial resolution of 0.25°x0.25° and at a monthly frequency between 1997 and 2022. Using this information, we identify and exclude from the sample plant-month-year observations where fire emissions are observed within 50 km of a power plant.

To account for other confounding factors, we also include in our dataset several meteorological variables derived from the Weather for Energy Tracker database (IEA and CMCC, 2022).[7] These variables provide monthly frequency information and correspond to the mean value observed within 50 km of each power plant. The meteorological variables are: temperature (°C at 2m), total precipita-

[5] https://sites.wustl.edu/acag/datasets/surface-pm2-5/

[6] https://www.geo.vu.nl/ gwerf/GFED/GFED4/

[7] https://www.iea.org/data-and-statistics/data-tools/weather-for-energy-tracker.

Figure 2: Combustion power plants, 50km radius, and $PM_{2.5}$ concentrations

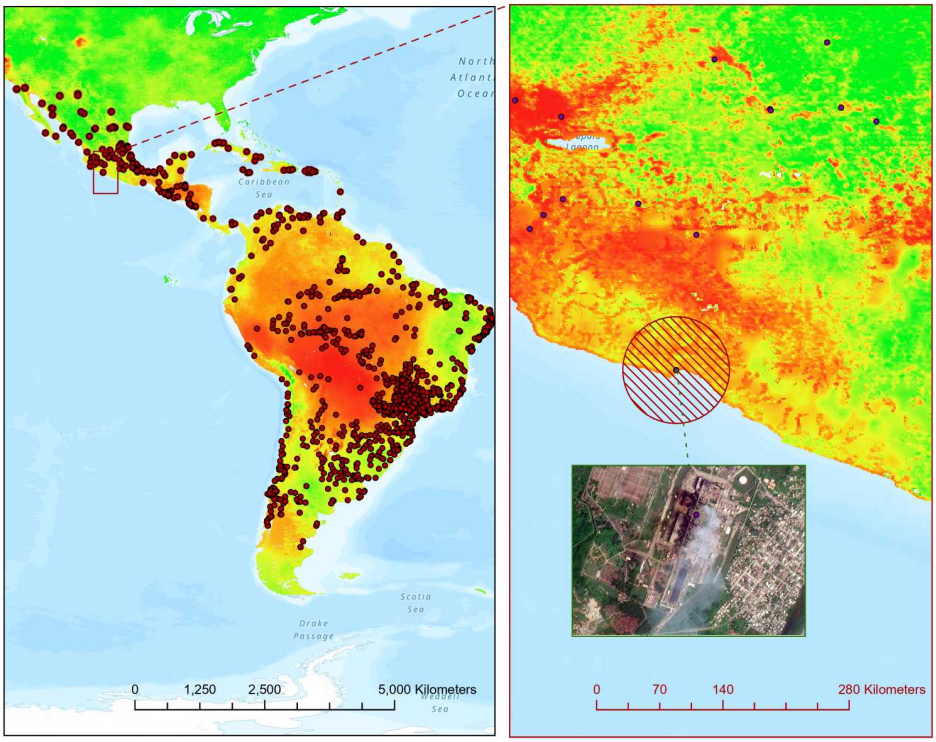

Notes: Dots represent combustion power plants (N = 1,835), hatched circles show the 50 km radius around each combustion power plant, and the color gradient indicates $PM_{2.5}$ concentrations ranging from low (green) to high (red). The right panel zooms into the coal power plant Plutarco Elías Calles in Mexico (October 2020) and shows its 50 km radius.

tion (mm/h), relative humidity (%), surface pressure (Pa), and wind speed (m/s at 10m and 100m). The definitions and source of these variables can be found in IEA (2022). Additionally, to account for changes in electricity demand related to meteorological conditions (e.g., heat waves), we include market-level measures of heating degree-days (HDD) and cooling degree-days (CDD) as part of our dataset. Following IEA guidelines we define HDD (°C days) with 18 °C reference and a 15 °C threshold. Similarly CDD (°C days) is defined with 18 °C reference and a 21 °C threshold. See IEA (2022) for further details.

To quantify exposure to excess $PM_{2.5}$ concentrations, we compute the population

residing within 50 km of combustion power plants. Specifically, we use modeled population at 100-meter spatial resolution available at five-year intervals from the Global Human Settlement Layer (GHSL) database[8] (European Commission, 2023). This dataset represents a significant advancement compared to prior attempts at modeling population distribution in space. It achieves this by refining raw census data into grid cells through the integration of remote-sensed imagery, specifically by utilizing the volume of residential areas. To avoid double counting the population in cases where the 50 km radius for different power plants overlaps, we partition these areas using a Thiessen method. We then compute the sum of the population residing in these areas in 2000, 2005, 2010, 2015, and 2020. We linearly interpolate the data obtained in the previous step for each power plant to create an annual frequency times series of the exposed population.

Additionally, to better characterize the population residing in proximity of a power plant, we use the Thiessen polygons derived previously and 2019 Human Development Index (HDI) data down-scaled to 0.1°x0.1° resolution from Sherman et al. (2023) to compute mean plant level HDI. We then compare the plant-level HDI with country-level HDI data from Smits and Permanyer (2019) to determine whether the population residing near power plants is systematically different.

Last, to study how excess $PM_{2.5}$ concentrations and exposure may change during the operational lifespan of power plants already in operation, we use runoff projections from 22 climate models from the Coupled Model Intercomparison Project Phase 6 (CMIP6). All these models provide runoff projections for the key Shared Socioeconomic Pathways (SSPs): SSP1-2.6, SSP2-4.5, and SSP3-7.0. Using this information on 66 future paths of runoff (22 models $\times$ 3 SSPs), we compute for each path and hydropower watershed the average runoff anomaly at monthly frequency between 2020 and 2060. The resulting dataset is then used to compute the evolution of the fraction of hydropower generation capacity affected by drought under the different models and SSPs. We also use the KC and Lutz (2017) population growth rate projections corresponding to each SSP to model the evolution of the population over the same time period.

[8] https://data.jrc.ec.europa.eu/dataset/9f06f36f-4b11-47ec-abb0-4f8b7b1d72ea

3 Methods and results

3.1 Empirical approach

We estimate the impacts of drought on average $PM_{2.5}$ concentrations around power plants with the following fixed effects regression:

$$PM_{icmy} = \beta HD_{cmy} + \mathbf{X}'_{icmy}\boldsymbol{\gamma} + \alpha_i + \alpha_{my} + \alpha_{cm} + \varepsilon_{icmy}, \tag{1}$$

where PM represents the average $PM_{2.5}$ (μg/m^3) within 50km of combustion power plant i in electricity market c in month m and year y.[9] HD_{cmy} is the market-level measure of hydrological drought, $\mathbf{X}$ is a vector of meteorological controls at the plant and market level, α_i are power plant fixed effects, α_{my} are month-by-year fixed effects, α_{cm} market-by-month fixed effects, and ε_{icmy} is the error term.

The parameter of interest is β, which measures the impact of hydrological droughts on $PM_{2.5}$ concentrations under the assumption that the shocks are exogenous given the controls. We account for time-invariant unobserved confounders using plant-level fixed effects, for time-varying unobserved common shocks using month-by-year fixed effects, and for market-specific seasonality using market-by-month fixed effects.

Because meteorological conditions related to hydrological droughts can also affect $PM_{2.5}$ concentrations, Equation 1 includes several meteorological controls including an indicator of local hydrological drought, temperature, total precipitation, relative humidity, surface pressure, and wind speed measured at a height of 10 and 100 meters. To also account for the effect of changes in electricity demand that may be correlated with hydrological drought conditions, we control for mean market-level HDD and CDD.

Moreover, in results presented in Figure 12, we relax the additivity and linearity assumptions of $\mathbf{X}'_{icmy}\boldsymbol{\gamma}$ in Equation 1 and consider a far richer set of controls, which includes up to third order polynomials of the controls in $\mathbf{X}_{icmy}$ as well as their pairwise interactions (up to 494 controls). We then use the post-double-selection estimator of Belloni et al. (2016) to test a series of alternative specifications that are more flexible than Equation 1 while remaining parsimonious.

[9] We classify plants as combustion if either the primary or secondary fuel type is coal, gas, oil, biomass, petcoke, or waste. Analogously, we classify plants as non-combustion if the fuel type is solar, wind, geothermal, or nuclear.

Because hydrological droughts can also affect $PM_{2.5}$ concentrations by increasing the likelihood of wildfires, we exclude from the sample plant-month observations where emissions from fires are observed. Because excluding these observations from the sample does not fully rule out the presence of $PM_{2.5}$ concentrations related to wildfires, in Figure 4, we also present the results of several robustness exercises that show that wildfires are not driving our results.[10]

We estimate Equation 1 and alternative specifications using Ordinary Least Squares. To allow for arbitrary patterns of correlation among $PM_{2.5}$ concentrations across space and over time, we cluster standard errors at the market level. Additionally, Figure A4 presents results where we derive standard errors under alternative assumptions.

3.2 Hydrological droughts lead to excess air pollution

We begin by estimating Equation 1 with our preferred measure of market-level hydrological drought, where HD_{cmy} is the fraction of hydropower generation capacity affected by drought (FHD). We define drought as experiencing an average negative runoff anomaly in the past three months. Figure 3 panel A plots point estimates and confidence intervals. The estimate presented in model 1 corresponds to the impact of the FHD. The estimated coefficient shows that $PM_{2.5}$ concentrations could increase by as much as 1.55 μg/m^3 in markets where FHD shifts from 0 to 100 percent. Because this large shift is seldom observed in our sample, in panel B, we plot the corresponding marginal effects, that is, the implied total $PM_{2.5}$ concentrations for different levels of FHD. The box plots provide an accurate representation of the distribution of the marginal effects given the FHD levels in our sample. The triangle markers represent $PM_{2.5}$ concentrations at the average FHD level. The panel reveals that $PM_{2.5}$ concentrations 50 km around power plants in the absence of droughts are in the order of 15.76 μg/m^3, they increase to 16.59 μg/m^3 at average levels of FHD, and can increase to up 17.31 μg/m^3 for the highest FHD levels observed in our sample. These results are quantitatively important as they indicate that there is an increase of roughly 0.83 μg/m^3 at average FHD levels. In panel A model 2 (dose-response), we plot the coefficients from an additional exercise where we estimate Equation 1 after discretizing the FHD vari-

[10] An alternative mechanism through which wildfire smoke could increase pollution is by reducing solar generation and increasing generation from combustion power plants (Gilletly et al., 2023). This mechanism is unlikely to be important in the region, as solar generation constitutes a small fraction of total generation during our sample period.

Figure 3: Effect of the fraction of hydropower generation affected by drought (FHD) on $PM_{2.5}$ concentrations

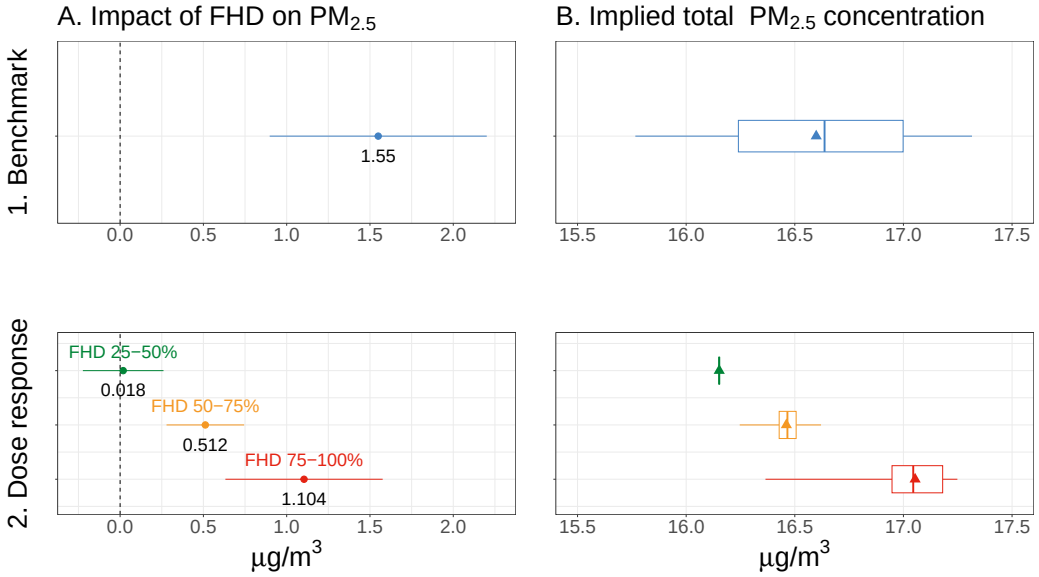

Notes: Panel A plots point estimates and 95 percent confidence intervals (CIs) of β in Equation 1. The CIs are derived from standard errors clustered at the market level. The benchmark model uses our preferred measure of hydrological drought FHD. The dose-response model shows estimates from an augmented version of Equation 1 where the FHD variable is discretized in four groups (less than 25, 25 to 50, 50 to 75, and greater than 75 percent). The reference group is FHD less than 25 percent. Panel B plots the distribution of implied total $PM_{2.5}$ concentrations, that is, the marginal effect plus the predicted level of $PM_{2.5}$ in the absence of droughts. The box represents the interquartile range, the whiskers report the minimum and maximum value, and the triangle indicates the average value.

able into four groups: FHD less than 25 percent, FHD 25 to 50 percent, FHD 50 to 75 percent, and FHD greater than 75 percent. These groups roughly correspond to the quartiles of the FHD variable. In the estimation, the reference group is FHD less than 25 percent. Consistent with the idea that hydrological droughts increase pollution by shifting generation to combustion power plants, we find that the impact on $PM_{2.5}$ increases as the fraction of hydropower plants experiencing drought grows. We also find that the increase in $PM_{2.5}$ is substantially larger when at least 50 percent of hydropower generation capacity is affected by drought.

Panel B further reveals that the implied $PM_{2.5}$ concentrations of the benchmark model are in a very similar range to that of the more flexible model presented in

the row labeled dose-response (16.14 to 17.24 μg/m^3). Given the similar results, we will focus on the more parsimonious benchmark model for the remainder of the paper.

3.3 Combustion power generation induced by drought drives excess air pollution

Having established that hydrological droughts lead to increased $PM_{2.5}$ concentrations, we turn our attention to considering and testing alternative mechanisms through which hydrological droughts might affect air pollution. Most prominently, droughts increase the likelihood of wildfires, one of the primary sources of $PM_{2.5}$ pollution (Burke et al., 2021, 2023; McClure and Jaffe, 2018; Childs et al., 2022). As noted in the data section, we excluded from the sample plant-month observations where we observe emissions from wildfires. This restricted sample lessens the concern that our results are driven by wildfires but does not entirely rule out this possibility as $PM_{2.5}$ pollution can be suspended in the atmosphere for several days and may travel for hundreds of kilometers. To address this issue and the related concern of other natural sources of $PM_{2.5}$ emissions like dust storms (Heft-Neal et al., 2020) also related to droughts, Figure 4 presents results from two placebo exercises (models 2 and 3).

In the first placebo exercise, we compute $PM_{2.5}$ concentrations within a 50 radius of non-combustion power plants (e.g., wind, solar, and nuclear) and exclude observations with combustion power plants within that radius. We then estimate Equation 1 using this sample. If fires or dust storms drive the excess air pollution, we should also expect to observe an increase in air pollution in this sample of non-combustion power plants. However, consistent with the idea that fires and dust storms are not the primary mechanism for the excess air pollution documented previously, we find that the impact of FHD on air pollution around non-combustion power plants is small and statistically indistinguishable from zero. One important caveat with the previous exercise is that the location of combustion and non-combustion power plants may differ systematically, and the resulting null effect may reflect the differences in geographic characteristics. To address this limitation, the second placebo exercise tests whether air pollution increased among combustion power plants in the years before they were operational. Once again, we cannot reject the null hypothesis that the impact of FHD on air pollution is different from zero. These placebo exercises indicate that wildfires and dust storms are unlikely to drive our results and that a more likely mechanism is

the shift in generation towards combustion power plants.

Figure 4: Placebo exercises

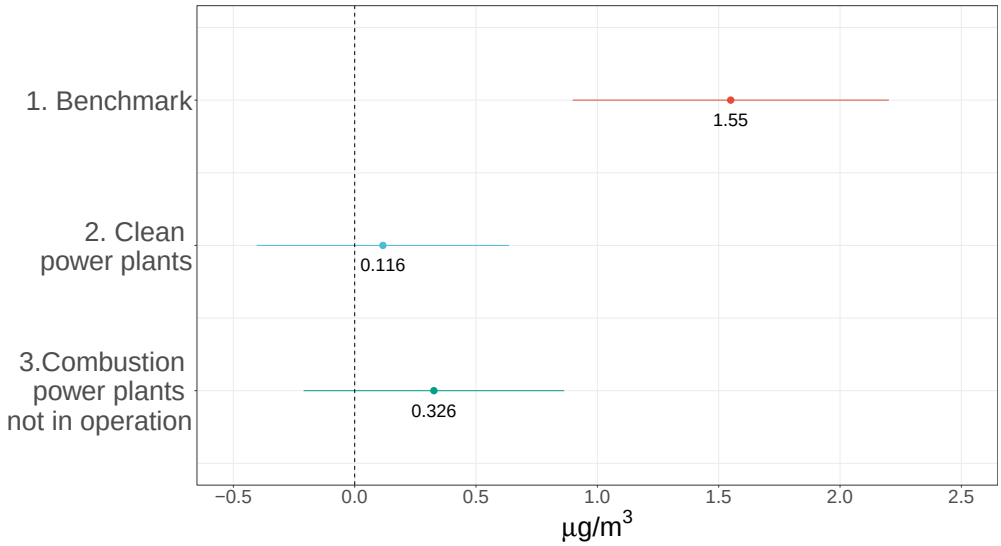

Notes: The figure plots point estimates and 95 percent confidence intervals (CIs) of β in Equation 1. The CIs are derived from standard errors clustered at the market level. All specifications use FHD as our preferred measure of hydrological drought (HD). Model 1 is our benchmark, reflecting the same estimate as model 1 in Figure 3, panel A. The second model presents an estimate derived from a sample that only includes non-combustion power plants (e.g., wind, solar, and nuclear). The sample further excludes plants with combustion power plants within a 50 km radius. The third model presents an estimate derived from a sample composed of combustion power plants in the period before they became operational.

3.4 Heterogeneous effects

Next, we conduct a series of exercises to document whether excess air pollution induced by hydrological drought varies with the characteristics of combustion power plants, such as their size and fuel source. In the plant size exercise, as measured by capacity, we follow the US Department of Energy definition and create an indicator variable for larger than 30 MW. We then augment Equation 1 by including an interaction term between the FHD variable and the size indicator variable. Analogously, we augment Equation 1 in the fuel source exercise by including an interaction term with an indicator variable for the fuel source type

(e.g., coal, gas, oil, biomass, or other). We then perform separate estimations of each augmented version of Equation 1 and compute the marginal effects, that is, the impact of FHD on $PM_{2.5}$ concentrations for each subgroup. Figure 5 plots the resulting point estimates and 95 percent confidence intervals. The figure reveals that hydrological droughts lead to excess air pollution in all subgroups, with the increase being substantially smaller for larger-capacity power plants (more than 30 MW) and for plants that use coal and gas as fuel.

There are several possible explanations for this pattern of results. One interpretation is that the largest increases in air pollution occur among power plants that are likely to have spare capacity. While we do not observe plant-level capacity factors in our data, baseload electricity generation is usually composed of large-capacity coal and gas power plants Sanders (2015). Since these plants are designed to run continuously near their maximum capacity, it is also reasonable that we observe a more limited adjustment in generation and, hence, pollution response to droughts. Another reason large baseload power plants have limited adjustment capacities during drought is that they tend to be more water-intensive than smaller power plants Sanders (2015). Smaller combustion power plants, to a larger extent, utilize air-cooling methods and tend to be composed of biomass and oil plants in our sample. In line with this, among all combustion power plants, we find the largest drought-induced pollution increase for biomass power plants, a well-known significant source of particle pollution.

We view this pattern of results as providing further supporting evidence in favor of the idea that hydrological droughts increase air pollution by shifting generation to combustion power plants.

4 The cost of drought-induced excess air pollution

4.1 Lives lost due to excess air pollution

To compute premature deaths, we combine a concentration-response function (CRF) with our estimate of excess $PM_{2.5}$ air pollution induced by drought and counts of exposed population. Our counterfactual calculation involves several steps. In the first step, we compute excess $PM_{2.5}$ air pollution by multiplying our benchmark estimate (Figure 3 panel A) by the observed FHD. The resulting market-by-month-year variable measures the additional air pollution observed in response to hydrological droughts shifting electricity generation to combustion

Figure 5: Effect of the fraction of hydropower generation affected by drought (FHD) on $PM_{2.5}$ concentrations, by subgroup

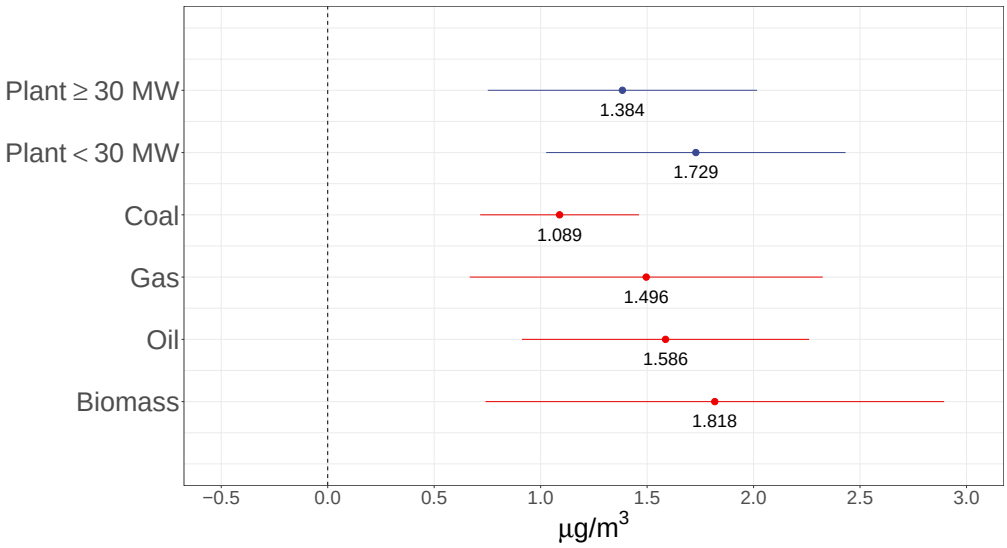

Notes: The figure plots point estimates and 95 percent confidence intervals (CIs). The CIs are derived from standard errors clustered at the market level. All specifications use FHD as the measure of hydrological drought (HD). In the first model (blue), we estimate an augmented version of Equation 1 where we interact the FHD variable with a binary indicator for plant capacity greater than 30 MW. In the second model (red), we perform an analogous exercise, but we interact the FHD variable with an indicator variable of the plant's fuel type. In all cases, we report the marginal effects, that is, the impact of FHD for each sub-group. The coefficient on plants greater or equal to 30 MW is statically different from the coefficient on plants smaller than 30 MW at the five percent level. The coefficient for plants that use coal is statically different from the coefficient for plants that use oil at the five percent level.

power plants.

In the second step, we transform excess air pollution into premature deaths using the CRF estimated by Deryugina et al. (2019). We prefer this CRF estimate because Deryugina et al. (2019) exploits variation in daily wind direction to establish the causal relationship between $PM_{2.5}$ concentrations and excess mortality. According to their CRF, a day of exposure to 1 µg/m^3 leads to 0.69 excess deaths per million U.S. adults 65 or older (Medicare beneficiaries). To use their CRF, we transform it to monthly frequency by multiplying it by 30.

In the third step, we compute the counts of the exposed population. Specifically,

for each combustion power plant, we compute the count of the population 65 or older residing within 50 km by multiplying the all-age population counts, described in the data section, by the fraction of the population 65 or older. Information on the fraction comes from World Bank (2023a) and is available at the country year level. Accordingly, this calculation assumes that the age distribution is uniform within countries.

In the fourth step, we derive counts of premature deaths at the plant-month-year level by multiplying the variables described in steps one to three. For ease of presentation, we aggregate this count of premature deaths to the LAC by year level.

Last, to account for uncertainty in our estimate of excess air pollution, in the first step, we draw our coefficient from a normal distribution with a mean equal to the estimated coefficient (1.55) and a standard deviation equal to the standard error (0.31). We then repeat 1,000 times steps one to four, taking a new draw each time.[11]

Figure 6 plots the evolution of drought-induced premature deaths in LAC. The spread of the box plot displayed each year results from the uncertainty in our estimation of excess $PM_{2.5}$ concentrations and the observed FHD. The figure reveals the scale of the cost for LAC, with median premature deaths per year ranging from 3,681 to over 10,610. In Figure A2 in the appendix, we show that using the CRFs from Liu et al. (2019) leads to median premature deaths per year that are in the order of 503 to 4,987. The CRFs from Liu et al. (2019) have the advantage of being derived for Chile and Mexico but have the disadvantage of not being causal CRFs.

Another important consideration is that our counts of premature deaths could underestimate the actual number of deaths if groups with lower socioeconomic status are disproportionately exposed and vulnerable to $PM_{2.5}$. There are several reasons why exposure might be higher among individuals with lower socioeconomic status, including a greater likelihood of residing near sources of $PM_{2.5}$ and engaging in outdoor occupations. Moreover, the adverse impact of $PM_{2.5}$ on health is exacerbated among the disadvantaged due to their comparatively lower baseline health status and more limited access to medical services.

[11] Specifically, we compute the number of premature deaths per plant-month-year for each draw by: 0.69 (CRF) $\times$ 30 (days) $\times$ FHD $\times$ draw of FHD coefficient from $\sim \mathcal{N}(1.55, 0.31)$ $\times$ exposed population 65 or older.

Figure 6: Premature deaths. Based on the concentration-response function of Deryugina et al. (AER, 2019) for adults 65 or older

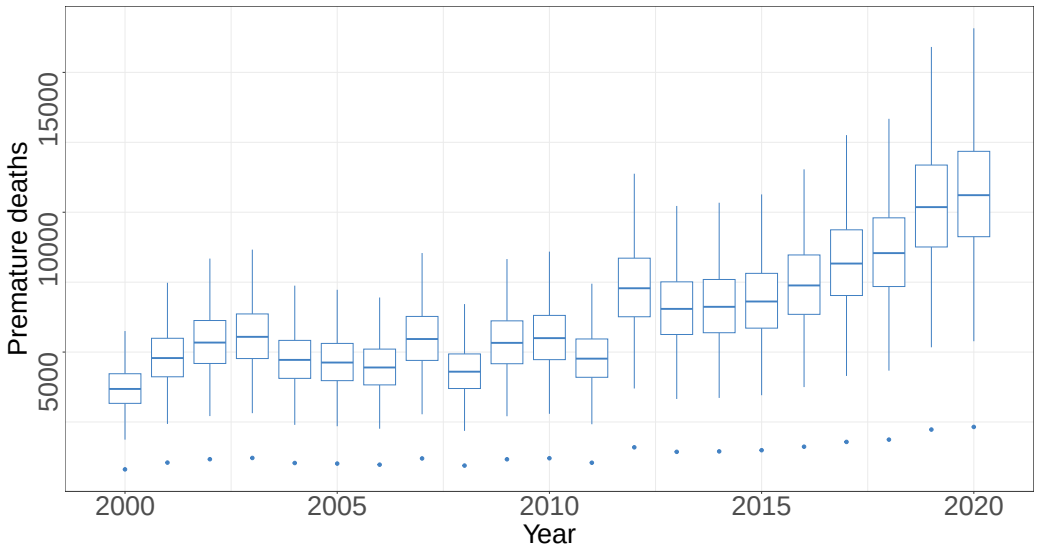

Notes: This figure plots the evolution of drought-induced premature deaths in LAC. Details of the calculation of premature deaths are presented in Section 4.1. The spread of the box plot displayed each year results from the uncertainty in our estimation of excess $PM_{2.5}$ concentrations and the value of the observed FHD. Dots represent outliers.

To descriptively assess in our setting whether the population residing near power plants tends to be worse off than the overall population, we use down-scaled Human Development Index (HDI) data from Sherman et al. (2023) to compute power plant level mean HDI relative to country-level HDI. As illustrated in Figure 7, in nearly four of every five combustion power plants, the population residing near the plant has a considerably lower relative level of HDI. Moreover, this pattern is systematic across all types of combustion power plants (i.e., coal, gas, oil, biomass). This finding is consistent with previous work on air quality and inequality, which has highlighted the correlation between poverty and exposure to $PM_{2.5}$ both across and within countries (e.g., Rentschler and Leonova, 2023; Jbaily et al., 2022). The association of lower HDI levels near combustion power plants can be a result of socioeconomic sorting into cheaper housing near industrial zones, siting decisions to place plants in areas with less political power, often coinciding with low-income

Figure 7: Combustion power plant HDI relative to country HDI

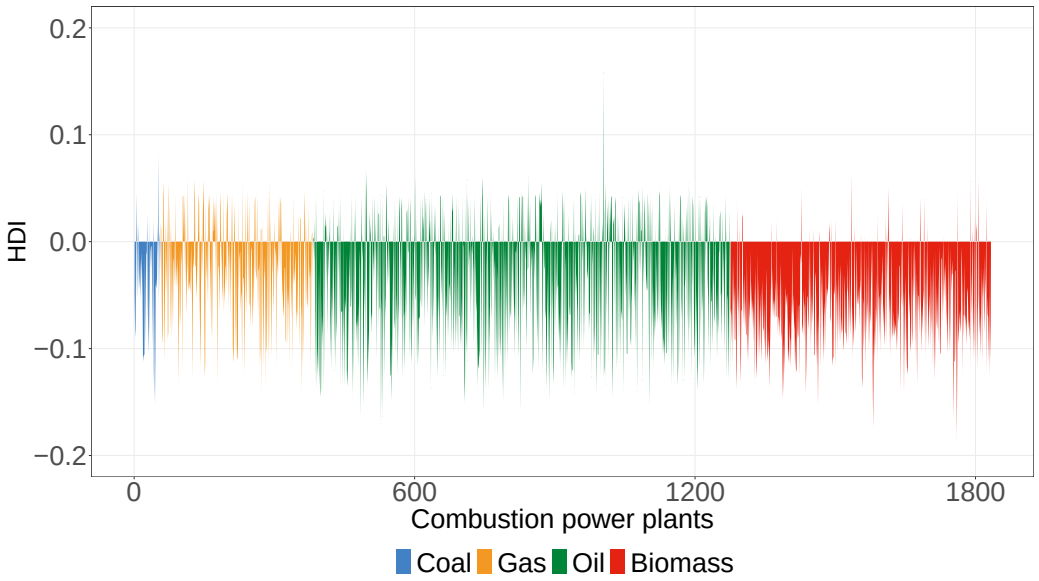

Notes: This figure plots for each combustion power plant the difference between the average Human Development Index (HDI) among the population residing within 50 km and the HDI of the country where the plant is located. The HDI was measured in 2019.

neighborhoods, or the adverse effects of past pollution exposure on HDI. Despite the varied reasons for this association, this exposure pattern is noteworthy because our CRFs do not capture the plausibly greater vulnerability for populations with lower HDI levels. Consequently, our counterfactual calculations of premature deaths are likely to underestimate the deaths caused by excess $PM_{2.5}$ in the region.

4.2 Value of lives lost due to excess air pollution

To monetize the cost of the lives lost previously documented, we calculate the Value of a Statistical Life (VSL) estimate at the country-year level in two steps. In the first step, we follow Banzhaf (2022) and compute a base VSL from a meta-meta-analysis of U.S. VSL estimates. In the second step, we follow Viscusi and Masterman (2017) and calculate an income-adjusted extrapolation for each country and year using our base VSL, the GNI per capita data from World Bank (2023b), and assuming that the income elasticity of the VSL is equal to

one. Next, we compute the monetized losses in 2019 U.S.$ by multiplying our estimates of premature deaths by the country and year-specific VSL estimates. Figure 8 plots the evolution of these drought-induced losses in LAC. The figure reveals that yearly median losses are in the order of $2.4 to $12 billion. An analogous exercise using the Liu et al. (2019) CRF shows median losses of $0.5 to $4.9 billion (Figure A3 in the appendix).

Figure 8: Value of statistical lives lost. Based on the concentration-response function of Deryugina et al. (AER, 2019) for adults 65 or older and extrapolated US VSL from Banzhaf (JBCA, 2022).

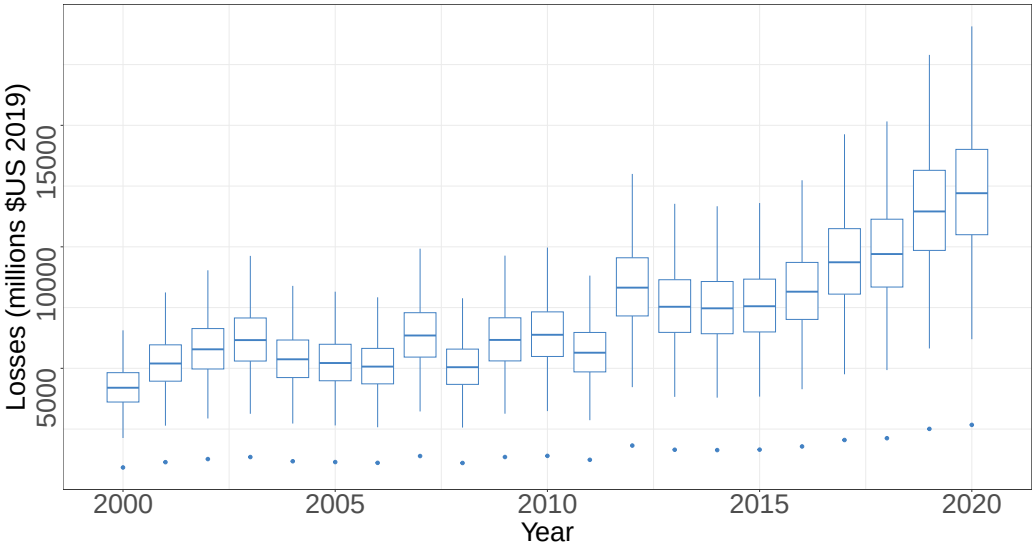

Notes: This figure plots the evolution of the losses from lives lost in LAC. Details of the calculation of premature deaths are presented in Section 4.2. The spread of the box plot displayed each year results from the uncertainty in our estimation of excess $PM_{2.5}$ concentrations and the value of the observed FHD. Dots represent outliers.

Importantly, these monetized longevity losses are significantly underestimating the total social cost of worsened air quality triggered by droughts. Our counterfactual simulations do not account for the fact that the absence of excess $PM_{2.5}$ would not only lead to health improvements that extend life but also increase the quality of life (Murphy and Topel, 2006). Additionally, our loss estimates do not account for non-health costs, such as effects on productivity and cognitive ability (Adhvaryu et al., 2022; Kahn and Li, 2020; Zivin and Neidell, 2012). Recent lit-

erature has shown that these non-health costs created by air pollution can be very considerable, with an increase in 1 $\mu g/m^3$ leading up to a 0.8 percent reduction in GDP (Dechezleprêtre et al., 2019). For all these reasons, our loss estimates should be interpreted as lower bounds.

5 The future cost of drought-induced excess air pollution

With an average commissioning year of 2003 and a lifespan of up to 60 years (Mills et al., 2017), the negative externality created by the combustion power plants in our sample could continue for four more decades. In this section, we quantify the possible paths of losses by combining our estimates with climate projections from 22 climate models from the CMIP6 under three Shared Socioeconomic Pathways (SSPs): SSP1-2.6 (low emissions), SSP2-4.5 (intermediate emissions), and SSP3-7.0 (high emissions). The SSPs are a set of scenarios and provide projections on several outcomes, including runoff, demographic changes, and economic growth.

In the first exercise, we quantify whether the hydropower plants are more likely to experience hydrological droughts, and we document the sub-regional heterogeneity in drought exposure. Specifically, for every climate model and SSP, we compute the percentage change in the average FHD between 2020 and 2059 relative to the FHD observed between 2000 and 2019. The result of this exercise for LAC is plotted in Figure 9 panel A. We summarize this information using box plots because we have 66 possible future paths (3 SSP $\times$ 22 models). Each box plot corresponds to one of the SSPs, and the variability of the box plot is determined by the distribution of projections given by the 22 climate models. The triangle marker represents the ensemble mean from the 22 models. For the region, most models indicate an increase in the fraction of hydropower generation affected by hydrological droughts. The ensemble mean suggests that the FHD will likely increase between 22 and 24 percent. The ranking in the FHD increase is consistent with higher-emission SPPs leading to a higher drought exposure. Still, the differences across SPPs will remain small by 2060.

Figure 9: Projected change in hydropower affected by drought 2020-2059 relative to 2000-2019, under different climate scenarios

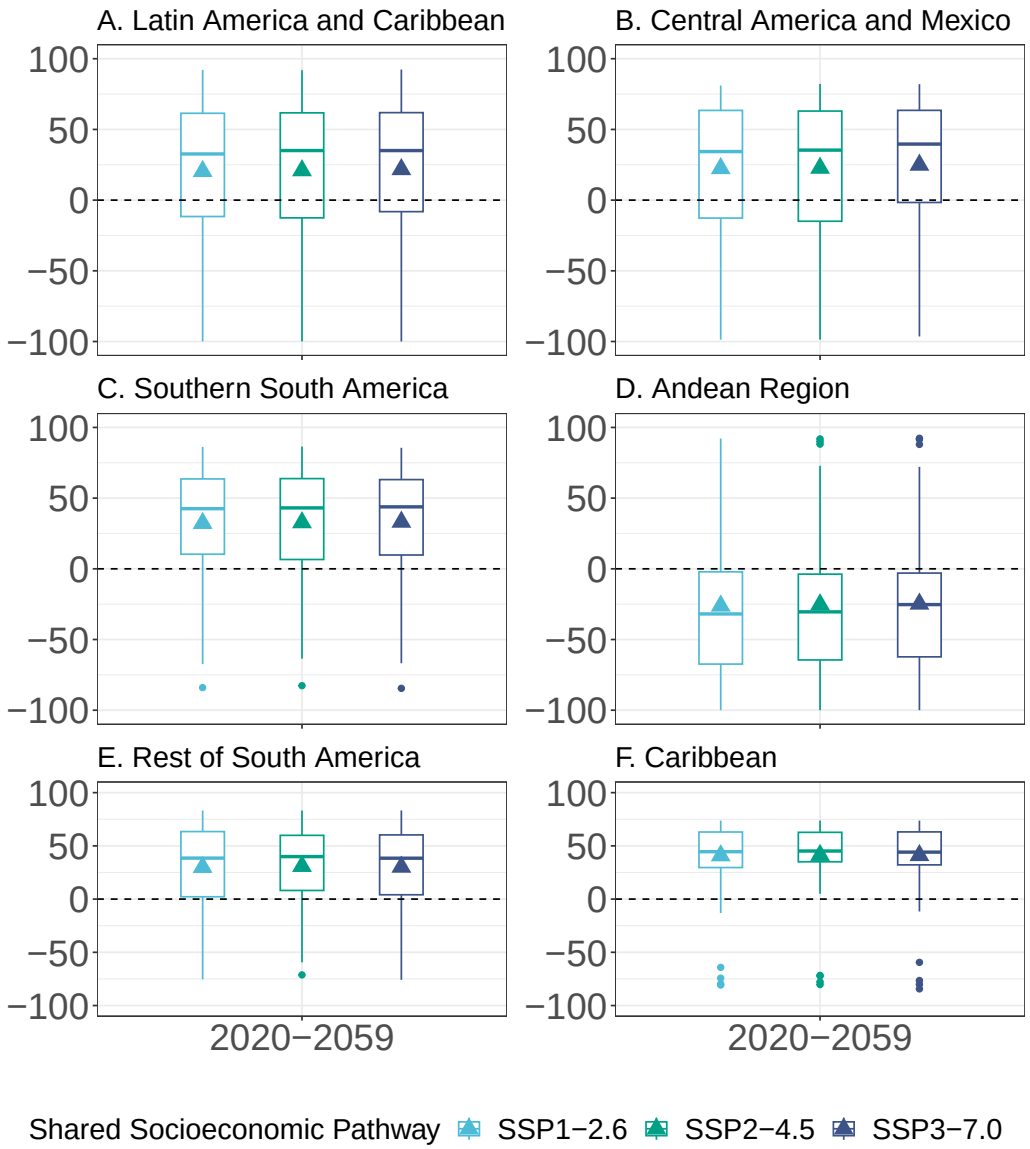

Notes: Computations based on 22 climate models from the CMIP 6. The spread of the box plots is determined by the distribution of projections given by the 22 climate models. Triangles represent the ensemble mean from the 22 models. Dots represent outliers. The overall sample is: A. Latin America and the Caribbean. The IEA sub-regions are: B. Central America and Mexico, C. Southern South America (Argentina, Bolivia, and Chile), D. Andean Region (Colombia, Ecuador, and Peru), E. Rest of South America (Brazil, Venezuela, Paraguay, and Uruguay), and F. Caribbean.

Next, we perform an analogous analysis for each IEA sub-region. The results from these exercises are presented in panels B to F. Nearly all sub-regions are expected to see an increase in FHD, with sub-regions like the Caribbean and Southern South America particularly hard hit. One notable exception is the Andean Region (Colombia, Ecuador, and Peru), which is expected to see a reduction in the FHD of roughly 25 percent. Given the location of the Andean Region and the anticipated evolution of hydrological droughts, this result highlights the potential that cross-border trade may hold in mitigating drought-induced air pollution.

In the second exercise, we project the evolution of premature deaths in LAC up to 2059. Specifically, we extend the premature deaths counterfactual calculation presented in Section 4.1 but compute excess air pollution using the runoff projections from the climate models instead of the observed runoff. We also allow for demographic changes using the demographic projections of the SSPs. The SSPs do not include projections on the evolution of electricity generation. However, because we expect the retirement schedule of combustion power plants to have significant implications for this exercise, we include information on possible retirements of combustion power plants by taking advantage of the region's IEA electricity generation scenarios and attaching the most closely aligned scenario to each SSP.

For SSP1-2.6, we use the Announced Pledges Scenario (APS). This scenario is described in IEA (2023) and is consistent with an expected temperature rise of 1.7 °C by 2100. This scenario outlines how total electricity generation by fuel type will evolve if countries fully honor existing pledges. This scenario is optimistic as it does not mirror what governments are doing but rather governments' aspirations. In this scenario, gas, coal, and oil power generation are expected to decline, while bioenergy generation is expected to increase. For the exercise, we omit the increase in bioenergy generation (no new plants are included) and use the information on the decline in generation from coal, gas, and oil to model the phase-out of combustion power plants. To present the most optimistic scenario for $PM_{2.5}$ reduction, we assume that plants with the largest exposed population are retired first to meet the pledges.

For the SSP2-4.5, we use the Stated Policies Scenario (STEPS). This scenario is described in IEA (2023) and is consistent with an expected temperature rise of 2.4 °C by 2100. This scenario does not assume the automatic attainment of aspirational energy targets but is built on the IEA's current assessment of the re-

gion's energy system's direction based on policies in place or announced. In this scenario, gas, coal, and oil power generation are phased out at a slower rate than in the previous scenario. As before, we omit the expected increase in bioenergy production from the calculation and assume that plants with the largest exposed population are phased out first.

For the SSP3-7.0, we construct the Reference Electricity Scenario (RES) that assumes no changes in the electricity sector. In this scenario, combustion power plants are not retired and remain the marginal electricity generation source to make up for the hydroelectricity shortfalls due to drought. This scenario is not the most pessimistic possible as we still assume that any growth in electricity generation is made up by clean energy generation. In all scenarios, we also assume that the concentration-response function is constant, thus ruling out other forms of adaptation, such as the reallocation of population away from power plants.

The results from this exercise are presented in Figure 10. The figure plots observed premature deaths and 66 premature death projections (3 SSP-electricity scenarios $\times$ 22 models). We plot a LOESS curve for the observed premature deaths and the projections under each SSP-electricity scenario to better visualize the overall trends. The figure reveals that while substantial uncertainty exists on the projected number of premature deaths, it is only in the most optimistic scenario (SPP1-2.6-APS), where we observe a flattening out of premature deaths at a level of roughly 5,000 deaths per year by 2060. This level is similar to that observed in the early 2000s. Scenarios that do not automatically assume that the region's pledges will be met show significant increases in premature deaths. In the most pessimistic scenario (SPP3-7.0-RES), the projected premature deaths are roughly six times larger, with as many as 30,000 deaths per year by 2060. These findings highlight that even if countries in the region follow up on their pledges, it will not be enough to fully mitigate premature deaths from drought-induced $PM_{2.5}$.

In the third exercise, we monetize the losses from premature death projections using the same methodology as in Section 4.2. We allow for adjustments to the VSL estimates based on the economic growth projections of each SSP. The results are presented in Figure 11. The figure reveals that losses from premature death increase or flatten out in all SSP-electricity scenarios. The ranking across scenarios is the same as before, with the losses increasing exponentially over time due to the effect of economic growth on the VSL estimates. Overall, these findings underscore the challenge of merely flattening out losses. Even if current pledges are met, fully mitigating damages will require further action. These actions can en-

Figure 10: Projected deaths from drought-induced $PM_{2.5}$

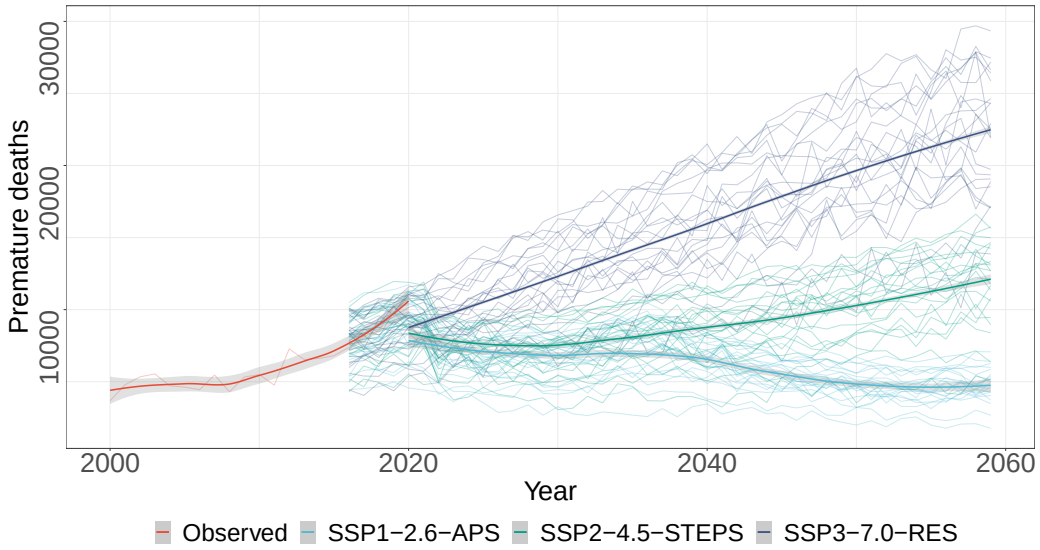

Notes: The figure plots the evolution of premature deaths in LAC. Between 2000 and 2020, it plots the average number of premature deaths. Details of this calculation are presented in Section 4.1. Between 2016 and 2059, it plots 66 projections of premature deaths (22 models $\times$ 3 SSP-electricity scenarios). These calculations follow the same methodology but use runoff projections from the climate models, demographic projections from the SSPs, and electricity scenarios from the IEA. To better visualize the overall trends, we also plot a LOESS curve for the observed premature deaths and for the projections under each SSP-electricity scenario.

compass more ambitious reductions in power generation from combustion power plants, including bioenergy, technological advancement that permits the reduction of emissions from power plants, or other forms of private and public adaptation that can reduce the exposure and vulnerability of the population to $PM_{2.5}$.

Figure 11: Projected monetized value of deaths from drought-induced $PM_{2.5}$

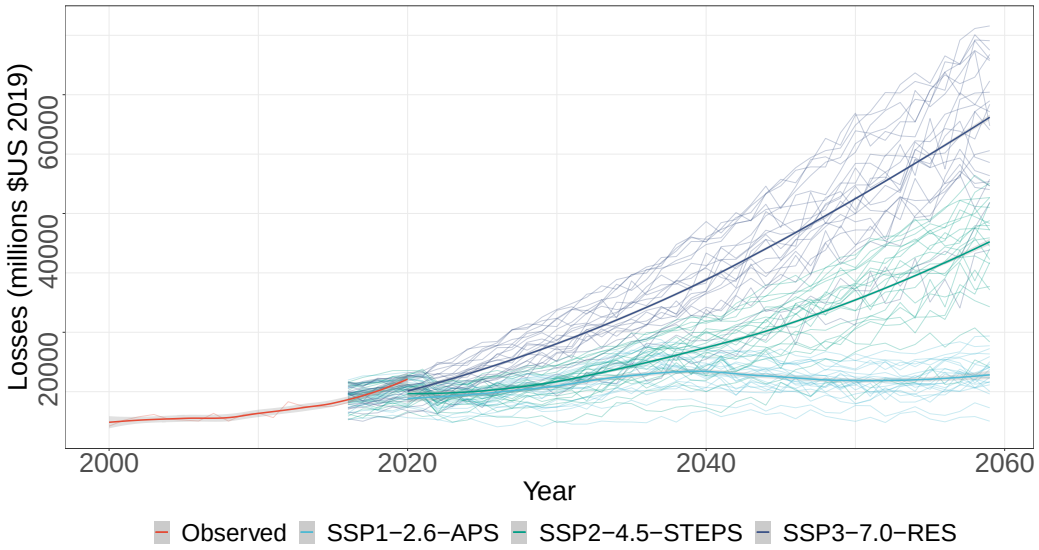

Notes: The figure plots the evolution of monetized losses from premature deaths in LAC. Between 2000 and 2020, it plots the average losses. Details of this calculation are presented in Section 4.2. Between 2016 and 2059, it plots 66 projections of losses (22 models $\times$ 3 SSP-electricity scenarios). These calculations follow the same methodology but use runoff projections from the climate models, demographic and economic growth projections from the SSPs, and electricity scenarios from the IEA. To better visualize the overall trends, we also plot a LOESS curve for the observed premature deaths and the projections under each SSP-electricity scenario.

6 Robustness checks

A key threat to the validity of our research design is the possibility that meteorological factors or changes in electricity demand may confound our estimates of the impact of hydrological droughts on $PM_{2.5}$. While we control for these factors in Equation 1, they enter our econometric model linearly, and we assume that their impact on $PM_{2.5}$ is independent of each other. We conduct several exercises to test that our results are robust to these assumptions.

Figure 12 plots point estimates and confidence intervals from these exercises. In the first exercise, we introduce into Equation 1 the meteorological and electricity demand controls in steps. As seen in models 1 to 3, we find a consistent and statistically significant effect of FHD on excess $PM_{2.5}$, albeit with the smallest point estimate on the specification that only includes fixed effects.

Figure 12: Robustness of estimates to alternative model specifications

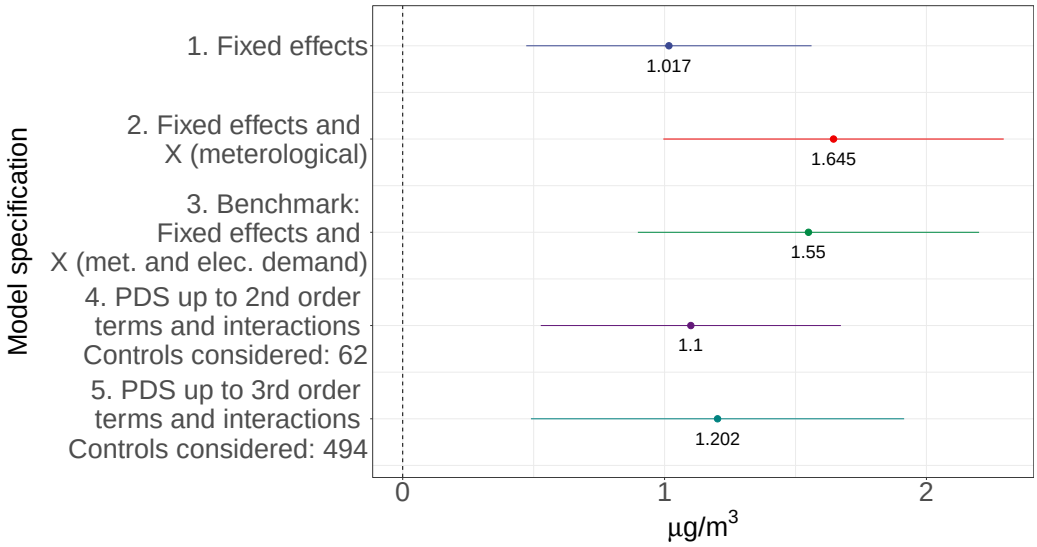

Notes: The figure plots point estimates and 95 percent confidence intervals (CIs) of β in Equation 1. The CIs are derived from standard errors clustered at the market level. All specifications use FHD as our preferred measure of hydrological drought (HD). Models 1 to 3 estimate specification 1 using OLS but introduce the controls in steps as described in the axis title. In models 4 and 5, we estimate Equation 1 using the post-double selection method of Belloni et al. (2014). The model specification and number of controls considered are specified in the axis title.

In the second exercise, we relax the assumption of linearity and additivity by including a far richer set of controls. Specifically, in model 4, we include second-order polynomials of each control variable (each element of the $\mathbf{X}$ vector) and all pairwise interactions (62 additional controls). Analogously, in model 5, we include third-order polynomials of each control variable and all pairwise interactions (494 additional controls). Simply including these controls in Equation 1 and performing the OLS estimation would make the assumption of including all relevant confounds more plausible, but it would come at the cost of lowering the precision of our estimates. To address this tradeoff, we use the more efficient post-double selection method of Belloni et al. (2016), which penalizes the models using a two-step LASSO procedure to select a subset of control variables that are important for predicting both $PM_{2.5}$ and FHD. This method allows us to guard against omitted-variables bias by considering these larger sets of controls while using a parsimonious model that produces valid inferential statements. As seen in the Figure, models 4 and 5 produce estimates of FHD that are statistically different from zero and whose 95 percent confidence intervals contain the point estimate from our benchmark specification (model 3). Accordingly, we conclude that our results are robust to the model specification.

Next, we test whether the inference of std errors used to construct confidence intervals is robust to alternative assumptions and methods. Figure A4 in the appendix presents results from these exercises. Model 1 plots the point estimate and confidence interval for the benchmark model. The confidence interval is constructed from standard errors clustered at the market (country) level. We present this type of confidence interval throughout the paper. Model 2 presents confidence sets derived using the wild cluster bootstrap method (Roodman et al., 2019). This method provides valuable complementary evidence as it is robust to violations of the standard large-sample assumptions necessary to derive cluster standard errors (e.g., large number clusters, homogeneous size). As the figure highlights, this more robust method produces a wider confidence set, but reassuringly, it shows that FHD remains statistically different from zero at conventional levels.

Another assumption necessary for clustered standard errors to be valid is that observations in different clusters are independent of each other. While this assumption is likely to hold in our setting, given that our clustering units (markets) are much larger than our observational units (plants), it is still possible for plants located on opposite sides of a cluster boundary to be affected by a correlated and unobserved shock. To account for this possibility and the resulting greater likelihood of type 1 errors, in models 3 and 4, we move away from using non-

overlapping clusters and compute Conley errors using the methodology of Colella et al. (2023). Following their recommendations, we assume a binary covariance matrix, fully account for temporal dependence by allowing the lag cutoff to equal the length of our panel, and present results with a narrow and wide distance cutoff (50 km and 5,000 km). The wide distance cutoff exceeds the length of Chile (the longest country in our sample). As seen in the figure, the confidence intervals derived from Conley errors (models 3 and 4) are much narrower than those of our benchmark (model 1), confirming in all cases that the estimate of FHD is statistically different from zero. These findings highlight that the confidence intervals used throughout the paper do a good job of quantifying the uncertainty associated with estimating FHD and that our conclusions are robust to alternative assumptions and methods for estimating standard errors.

We now turn our attention to testing whether our results are robust to using alternative variable definitions. We begin with the definition of hydrological drought used to compute the FHD variable. Throughout the paper, we have defined that a hydropower plant experiences a hydrological drought when we observe an average negative runoff anomaly over the past three months. To assess the importance of this definition as described in the data section, we compute alternative versions of the FHD variable where we define drought as observing average negative runoff anomalies over averaging windows of length 1, 6, 9, and 12 months. Figure A5 in the appendix reports the results from separately estimating Equation 1 using each version of the FHD. Panel A presents point estimates and confidence intervals. Panel B plots the implied total $PM_{2.5}$ concentrations ($PM_{2.5}$ concentrations in the absence of droughts plus the marginal effect). The figure shows that estimates of the FHD are similar for all definitions, albeit slightly larger when using shorter averaging windows. This finding is important because it highlights that even short-run droughts can considerably increase $PM_{2.5}$ concentrations in LAC. This finding is consistent with the widespread presence of small hydropower plants in the region, for whom even short-run changes in water availability imply reduced generation capacity.

We also test and find similar results using alternative ways of aggregating our watershed measure identifying hydropower plants affected by drought to the market level. The first type of exercise sequentially estimates Equation 1 using alternative versions of our preferred market-level measure, the fraction of hydropower generation affected by drought (FHD). The results from these exercises are reported in figure A6 in the appendix. Panels A and B are analogous to those of the previous figure. Model 1 reports the benchmark estimate. Model 2 uses an alternative ver-

sion of FHD that uses an arithmetic average instead of weighting by generation capacity. Model 3 computes the FHD as a fraction of overall generation instead of a fraction of hydropower generation. Model 4 allows for regional markets and computes the FHD, assuming that markets with small amounts of cross-border trade are fully integrated.[12] Model 5 performs the same calculation of the FHD as model 4 but uses an arithmetic average instead of weighting by generation capacity. Models 6 and 7 test the impact of FHD when we use more severe definitions of drought. In these cases, we compute the FDH either assuming that droughts occur when mean runoff anomalies are less than minus one standard deviation or runoff anomalies or when they are less than the median of negative anomalies. In model 8, we also verify that our results are robust to measuring $PM_{2.5}$ in a closer vicinity of combustion power plants (10 km). As seen in the figure, we find very similar results across models. While in panel A, some versions of the FHD lead to re-scaled and, in some cases, larger point estimates, panel B shows that the implied total $PM_{2.5}$ concentrations are nearly identical. The only exception is model 8, which, as expected, highlights that $PM_{2.5}$ concentrations are higher near combustion power plants.

The second type of exercise also aims to assess the robustness of the results to alternative market-level measures of hydrological drought. However, it focuses on measures that directly gauge the intensity of droughts. Figure A7 in the appendix presents results from these exercises. Panels A and B are analogous to those of the previous figure. We begin by computing the mean runoff anomaly among hydropower plants for each market. For ease of presentation, we convert this measure to standard deviation units and estimate Equation 1 using this variable in place of HD. We are particularly interested in negative runoff anomalies as they represent periods when water availability is below normal. As seen in model 1 panel A, a one-standard-deviation negative runoff anomaly leads to an increase of 0.36 $\mu g/m^3$. As shown in panel B, this estimate also implies that an average negative runoff anomaly leads to $PM_{2.5}$ concentration of 16.86 $\mu g/m^3$. This concentration level is very similar to the level implied by our benchmark specification estimate (16.59 $\mu g/m^3$ at the average FHD). To test whether negative and positive runoff anomalies have symmetric effects on $PM_{2.5}$, in model 2, we re-estimate Equation 1 but allow for a spline with a kink at zero. That is, we allow the slope coefficient to differ for positive and negative runoff anomalies. The estimates in

[12] Specifically, we compute the FDH considering that the following countries are part of larger regional markets. Market 1: Colombia, Ecuador, and Venezuela. Market 2: Brazil, Uruguay, Paraguay. Market 3: Central America.

panel A, while of a similar magnitude, indicate that one-standard-deviation negative runoff anomaly (drought) leads to a larger increase (0.44 μg/m^3) in $PM_{2.5}$ than the decrease in $PM_{2.5}$ that one-standard-deviation positive runoff anomalies would generate (-0.31 μg/m^3). This asymmetric result is important because it highlights that the externality created by drought periods cannot be offset by downpour periods. The smaller effect of positive runoff anomalies is consistent with the idea that infrastructure and operational limitations may restrict the ability of hydropower plants to fully harness downpour periods to increase generation. Next, in models 3 to 5, we compute for each market the mean runoff anomaly among all power plants. This change in the measure allows us to bring to the analysis a few markets without hydropower generation. In model 3, we estimate Equation 1 using this new measure and this slightly larger sample. In model 4, we restrict the sample to markets with limited hydropower capacity (less than 20 percent of overall generation). Finally, in model 5, we restrict the sample to markets reliant on hydropower (20 percent or more of overall generation). The figure shows that hydrological droughts affecting markets reliant on hydropower drive the increase in $PM_{2.5}$. Importantly, consistent with our mechanism, we also fail to find evidence of hydrological droughts leading to excess $PM_{2.5}$ in markets where hydropower plays a limited role in electricity generation.

7 Conclusion

We conduct the first region-wide study documenting how hydrological droughts lead to excess $PM_{2.5}$ by shifting generation from hydropower to combustion power plants. Our findings provide robust evidence showing that even short-run hydrological droughts generate a significant externality. At average levels of the fraction of hydropower generation affected by drought (FHD), we find increases in $PM_{2.5}$ in the order of 0.83 $\mu g/m^3$, which brings mean $PM_{2.5}$ concentrations around combustion power plants to roughly 16.59 $\mu g/m^3$.

We also provide several pieces of supporting evidence for our mechanism. These include showing the existence of a dose-response relationship between the FHD and excess $PM_{2.5}$, with placebos ruling out ruling alternative mechanisms such as wildfires or dust storms, and showing that the increase in $PM_{2.5}$ is driven by combustion power plants that are likely less-water intensive and have spare capacity. We conclude from this evidence that our estimate of excess $PM_{2.5}$ represents the additional air pollution created by the shift to combustion power plants triggered by hydrological droughts.

The public health implications of the shift in electricity generation are significant. Counterfactual calculations that build on our estimates of excess $PM_{2.5}$ and concentration-response function from the literature indicate that worsening air quality leads to up to 10,000 premature deaths annually. Making conservative assumptions on the value of statistical life, the monetized losses of these deaths are in the order of $12 billion (constant 2019 USD).

Coupling our counterfactual calculations with projections from climate and demographic models and stylized electricity sector scenarios shows that these losses will continue in the absence of adaptation over the next four decades. Another important finding of these projections is the considerable sub-regional heterogeneity, with most of the hydropower generation in LAC expected to experience increased water stress, with the exception of the Andean region.

Our findings have several important policy implications. First, we document a previously unaccounted-for cost of a drought-induced shift in electricity generation, accentuating the benefit of implementing demand-side management interventions that can help mitigate this shift in the short term. Second, by quantifying the externality, we also offer valuable input to the cost-benefit analysis of within-market infrastructure investments capable of reducing excess $PM_{2.5}$ over a longer time horizon, such as energy storage facilities. Third, by highlighting this cost and the

considerable sub-regional variation in hydropower exposure to drought, we bolster the case that increasing regional interconnection may provide an effective way to improve the reliability of clean energy and reduce air pollution. Fourth, because excess $PM_{2.5}$ falls disproportionately among those with lower socioeconomic status, we highlight that policy makers can lessen socioeconomic inequalities by addressing this externality.

Last, this analysis has three important caveats concerning the size of the externality and suggests that our loss estimates should be interpreted as lower bounds. First, our counterfactual calculations do not account for the disproportionate exposure to excess $PM_{2.5}$ by groups with lower socioeconomic status, whose increased vulnerability will likely lead to additional premature deaths in the region. Second, our estimates do not account for the costs created by excess $PM_{2.5}$ on other outcomes such as quality of life and productivity. Third, our estimates do not consider the cost of drought-induced excess emissions of other local or global pollutants, which have a wide range of environmental, health, and economic consequences. Notwithstanding the potential for even larger losses in LAC, this paper documents how the existing energy generation infrastructure and droughts interact to create a considerable health burden. This burden is poised to persist and potentially worsen without energy policies that account for the electricity-water nexus.

References

Adhvaryu, A., Kala, N., and Nyshadham, A. (2022). Management and shocks to worker productivity. *Journal of Political Economy*, 130(1):1–47.

Auffhammer, M. (2018). Quantifying economic damages from climate change. *Journal of Economic Perspectives*, 32(4):33–52.

Banzhaf, H. S. (2022). The value of statistical life: A meta-analysis of meta-analyses. *Journal of Benefit-Cost Analysis*, 13(2):182–197.

Banzhaf, S., Ma, L., and Timmins, C. (2019). Environmental justice: The economics of race, place, and pollution. *Journal of Economic Perspectives*, 33(1):185–208.

Belloni, A., Chernozhukov, V., and Hansen, C. (2014). Inference on treatment effects after selection among high-dimensional controls. *Review of Economic Studies*, 81(2):608–650.

Belloni, A., Chernozhukov, V., Hansen, C., and Kozbur, D. (2016). Inference in high-dimensional panel models with an application to gun control. *Journal of Business & Economic Statistics*, 34(4):590–605.

Burke, M., Childs, M. L., De la Cuesta, B., Qiu, M., Li, J., Gould, C. F., Heft-Neal, S., and Wara, M. (2023). Wildfire influence on recent US pollution trends. Working Paper 30882, National Bureau of Economic Research.

Burke, M., Driscoll, A., Heft-Neal, S., Xue, J., Burney, J., and Wara, M. (2021). The changing risk and burden of wildfire in the United States. *Proceedings of the National Academy of Sciences*, 118(2):e2011048118.

Byers, L., Friedrich, J., Hennig, R., Kressig, A., Li, X., McCormick, C., and Valeri, L. M. (2018). A global database of power plants. *World Resources Institute*, 18.

Childs, M. L., Li, J., Wen, J., Heft-Neal, S., Driscoll, A., Wang, S., Gould, C. F., Qiu, M., Burney, J., and Burke, M. (2022). Daily local-level estimates of ambient wildfire smoke PM2.5 for the contiguous US. *Environmental Science & Technology*, 56(19):13607–13621.

Clay, K., Lewis, J., and Severnini, E. (2016). Canary in a coal mine: Infant mortality, property values, and tradeoffs associated with mid-20th century air pollution. Working Paper 22155, National Bureau of Economic Research.

Cohen, A. J., Brauer, M., Burnett, R., Anderson, H. R., Frostad, J., Estep, K., Balakrishnan, K., Brunekreef, B., Dandona, L., Dandona, R., et al. (2017). Estimates and 25-year trends of the global burden of disease attributable to ambient air pollution: an analysis of data from the Global Burden of Diseases Study 2015. *The Lancet*, 389(10082):1907–1918.

Colella, F., Lalive, R., Sakalli, S. O., and Thoenig, M. (2019). Inference with arbitrary clustering. IZA Discussion Paper No. 12584, IZA - Institute of Labor Economics.

Colella, F., Lalive, R., Sakalli, S. O., and Thoenig, M. (2023). acreg: Arbitrary correlation regression. *The Stata Journal*, 23(1):119–147.

Dechezleprêtre, A., Rivers, N., and Stadler, B. (2019). The economic cost of air pollution: Evidence from Europe. OECD Economics Department Working Papers No. 1584, OECD.

Deryugina, T., Heutel, G., Miller, N. H., Molitor, D., and Reif, J. (2019). The mortality and medical costs of air pollution: Evidence from changes in wind direction. *American Economic Review*, 109(12):4178–4219.

Dockery, D. W., Pope, C. A., Xu, X., Spengler, J. D., Ware, J. H., Fay, M. E., Ferris Jr, B. G., and Speizer, F. E. (1993). An association between air pollution and mortality in six US cities. *New England Journal of Medicine*, 329(24):1753–1759.

European Commission (2023). GHSL Data Package 2023. Technical report, Publications Office of the European Union, Luxembourg.

Eyer, J. and Wichman, C. J. (2018). Does water scarcity shift the electricity generation mix toward fossil fuels? Empirical evidence from the United States. *Journal of Environmental Economics and Management*, 87:224–241.

Fraenkel, R., Zivin, J. G., and Krumholz, S. (2024). The coal transition and its implications for health and housing values. *Land Economics*, 100(1):51–65.

Gilletly, S. D., Jackson, N. D., and Staid, A. (2023). Evaluating the impact of wildfire smoke on solar photovoltaic production. *Applied Energy*, 348:121303.

Heft-Neal, S., Burney, J., Bendavid, E., Voss, K. K., and Burke, M. (2020). Dust pollution from the Sahara and African infant mortality. *Nature Sustainability*, 3(10):863–871.

Herrera-Estrada, J. E., Diffenbaugh, N. S., Wagner, F., Craft, A., and Sheffield, J. (2018). Response of electricity sector air pollution emissions to drought conditions in the western United States. *Environmental Research Letters*, 13(12):124032.

IEA (2021). *Climate Impacts on Latin American Hydropower*. International Energy Agency, Paris, Paris.

IEA (2022). *Weather for Energy Tracker: Users guide*. International Energy Agency, Paris.

IEA (2023). *Latin America Energy Outlook 2023*. International Energy Agency, Paris.

IEA and CMCC (2022). Weather for Energy Tracker database, License: Creative Commons CC BY-NC-ND 3.0 IGO.

Jbaily, A., Zhou, X., Liu, J., Lee, T.-H., Kamareddine, L., Verguet, S., and Dominici, F. (2022). Air pollution exposure disparities across US population and income groups. *Nature*, 601(7892):228–233.

Kahn, M. E. and Li, P. (2020). Air pollution lowers high skill public sector worker productivity in China. *Environmental Research Letters*, 15(8):084003.

KC, S. and Lutz, W. (2017). The human core of the shared socioeconomic pathways: Population scenarios by age, sex and level of education for all countries to 2100. *Global Environmental Change*, 42:181–192.

Lehner, B. and Grill, G. (2013). Global river hydrography and network routing: baseline data and new approaches to study the world's large river systems. *Hydrological Processes*, 27(15):2171–2186.

Liu, C., Chen, R., Sera, F., Vicedo-Cabrera, A. M., Guo, Y., Tong, S., Coelho, M. S., Saldiva, P. H., Lavigne, E., Matus, P., et al. (2019). Ambient particulate air pollution and daily mortality in 652 cities. *New England Journal of Medicine*, 381(8):705–715.

MacKinnon, J. G. and Webb, M. D. (2017). Wild bootstrap inference for wildly different cluster sizes. *Journal of Applied Econometrics*, 32(2):233–254.

McClure, C. D. and Jaffe, D. A. (2018). US particulate matter air quality improves except in wildfire-prone areas. *Proceedings of the National Academy of Sciences*, 115(31):7901–7906.

Mills, A. D., Wiser, R. H., and Seel, J. (2017). Power plant retirements: Trends and possible drivers. Technical report, Lawrence Berkeley National Lab (LBNL), Berkeley, CA.

Murphy, K. M. and Topel, R. H. (2006). The value of health and longevity. *Journal of Political Economy*, 114(5):871–904.

Pope III, C. A., Burnett, R. T., Thun, M. J., Calle, E. E., Krewski, D., Ito, K., and Thurston, G. D. (2002). Lung cancer, cardiopulmonary mortality, and long-term exposure to fine particulate air pollution. *JAMA*, 287(9):1132–1141.

Pope III, C. A., Ezzati, M., and Dockery, D. W. (2009). Fine-particulate air pollution and life expectancy in the United States. *New England Journal of Medicine*, 360(4):376–386.

Qiu, M., Ratledge, N., Azevedo, I. M., Diffenbaugh, N. S., and Burke, M. (2023). Drought impacts on the electricity system, emissions, and air quality in the western United States. *Proceedings of the National Academy of Sciences*, 120(28):e2300395120.

Rentschler, J. and Leonova, N. (2023). Global air pollution exposure and poverty. *Nature Communications*, 14(1):4432.

Roodman, D., Nielsen, M. Ø., MacKinnon, J. G., and Webb, M. D. (2019). Fast and wild: Bootstrap inference in stata using boottest. *The Stata Journal*, 19(1):4–60.

Sanders, K. T. (2015). Critical review: Uncharted waters? The future of the electricity-water nexus. *Environmental science & technology*, 49(1):51–66.

Sherman, L., Proctor, J., Druckenmiller, H., Tapia, H., and Hsiang, S. M. (2023). Global High-Resolution Estimates of the United Nations Human Development Index Using Satellite Imagery and Machine-learning. Working Paper 31044, National Bureau of Economic Research.

Smits, J. and Permanyer, I. (2019). The subnational human development database. *Scientific data*, 6(1):1–15.

Timilsina, G., Deluque Curiel, I., and Chattopadhyay, D. (2021). How Much Does Latin America Gain from Enhanced Cross-Border Electricity Trade in the Short Run? *World Bank Policy Research Working Paper*, (9692).

Van Der Werf, G. R., Randerson, J. T., Giglio, L., Van Leeuwen, T. T., Chen,

Y., Rogers, B. M., Mu, M., Van Marle, M. J., Morton, D. C., Collatz, G. J., et al. (2017). Global fire emissions estimates during 1997–2016. *Earth System Science Data*, 9(2):697–720.

Van Donkelaar, A., Hammer, M. S., Bindle, L., Brauer, M., Brook, J. R., Garay, M. J., Hsu, N. C., Kalashnikova, O. V., Kahn, R. A., Lee, C., et al. (2021). Monthly global estimates of fine particulate matter and their uncertainty. *Environmental Science & Technology*, 55(22):15287–15300.

Viscusi, W. K. and Masterman, C. J. (2017). Income elasticities and global values of a statistical life. *Journal of Benefit-Cost Analysis*, 8(2):226–250.

Weichenthal, S., Pinault, L., Christidis, T., Burnett, R. T., Brook, J. R., Chu, Y., Crouse, D. L., Erickson, A. C., Hystad, P., Li, C., et al. (2022). How low can you go? Air pollution affects mortality at very low levels. *Science Advances*, 8(39):eabo3381.

WHO (2021). *WHO global air quality guidelines: particulate matter (PM2.5 and PM10), ozone, nitrogen dioxide, sulfur dioxide and carbon monoxide*. World Health Organization.

World Bank (2023a). World development indicators: Fraction of population 65 or older. Accessed on May 17, 2023.

World Bank (2023b). World Development Indicators: GNI per capita, Atlas method. Accessed on May 17, 2023.

Zivin, J. G. and Neidell, M. (2012). The impact of pollution on worker productivity. *American Economic Review*, 102(7):3652–3673.

APPENDIX

A Supplementary Figures

Figure A1: Runoff anomalies over time

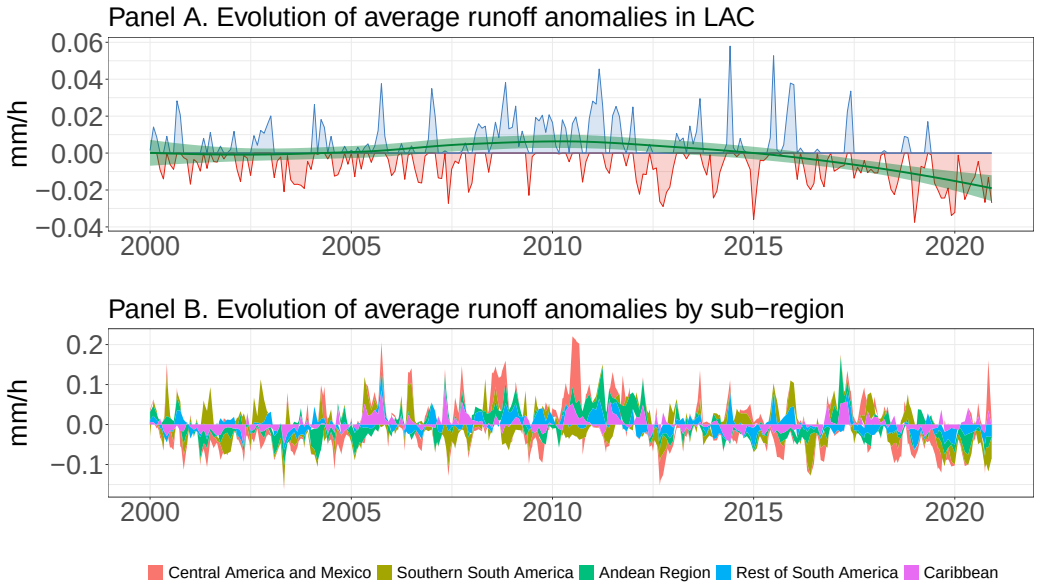

Notes: Panel A shows the regional monthly runoff anomalies. The blue-shaded areas represent positive runoff anomalies. The red-shaded areas represent negative runoff anomalies. To better visualize the trend over this period, we also plot a LOESS curve in green. Panel B shows monthly runoff anomalies by IEA sub-region. The sub-regions are: Central America and Mexico, Southern South America (Argentina, Bolivia, and Chile), Andean Region (Colombia, Ecuador, and Peru), Rest of South America (Brazil, Venezuela, Paraguay, and Uruguay), and Caribbean.

Figure A2: Premature deaths. Based on the concentration-response function of Liu et al. (NEJM, 2019)

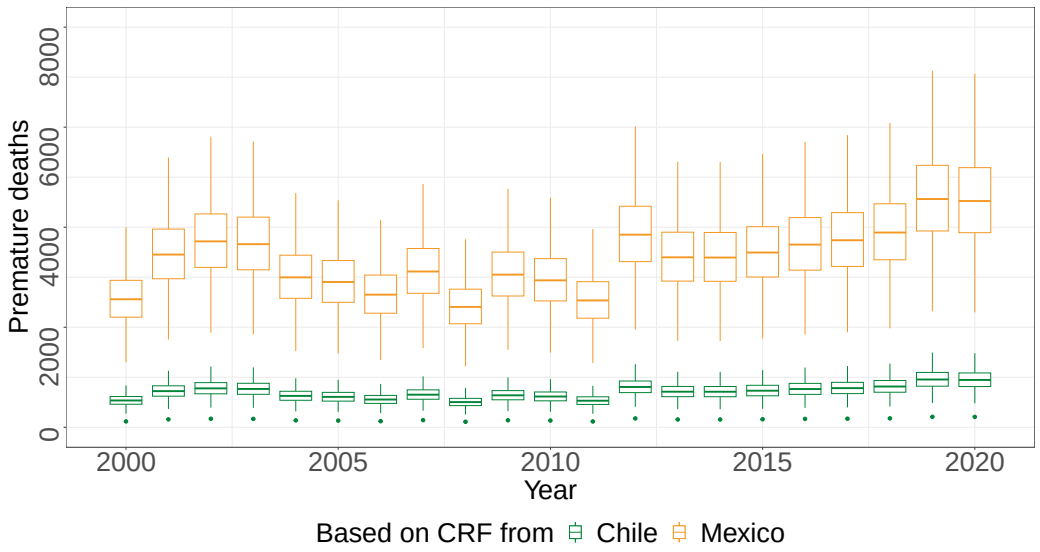

Notes: This figure plots the evolution of drought-induced premature deaths in LAC. The calculation based on the Mexico CRF is as follows. For each draw, we compute premature deaths per plant-month-and year using: 0.00129 (CRF) $\times$ 30 (days) $\times$ FHD $\times$ draw of FHD coefficient from $\sim \mathcal{N}(1.55, 0.31)$ $\times$ daily mortality rate $\times$ exposed population. We then aggregate to the LAC year level and repeat 1,000 times. The computation based on the Chile CRF is analogous, but the CRF takes the value of .00027. The spread of the box plot displayed each year results from the uncertainty in our estimation of excess $PM_{2.5}$ concentrations and the value of the observed FHD. Dots represent outliers.

Figure A3: Value of statistical lives lost. Based on the concentration-response function of Liu et al. (NEJM, 2019) and extrapolated US VSL from Banzhaf (JBCA, 2022)

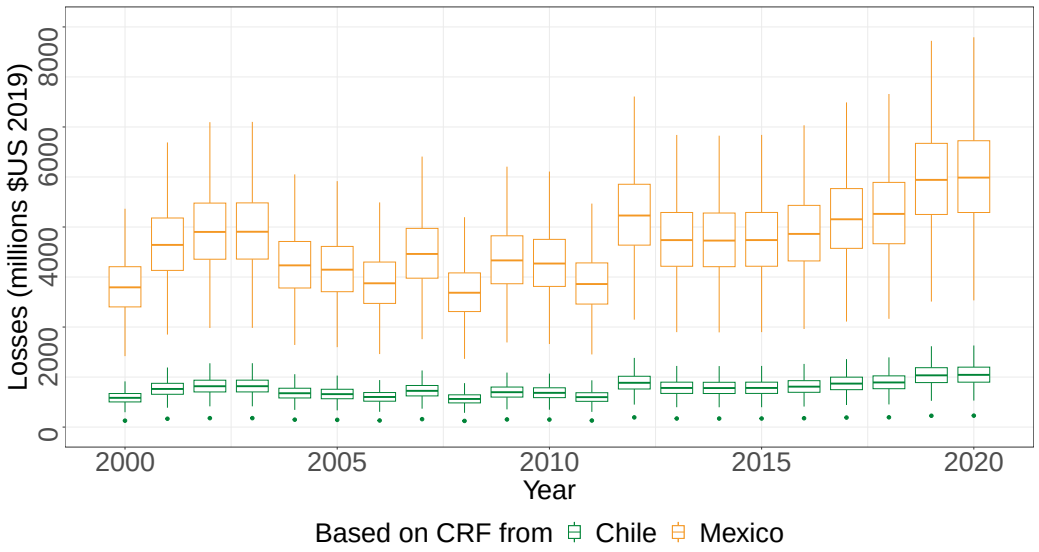

Notes: This figure plots the evolution of the losses from lives lost in LAC. To monetize the cost of the lives lost presented in Figure A2, we follow a procedure analogous to the one described in Section 4.2. The spread of the box plot displayed each year results from the uncertainty in our estimation of excess $PM_{2.5}$ concentrations and the value of the observed FHD. Dots represent outliers.

Figure A4: Robustness of estimates to std errors under alternative assumptions

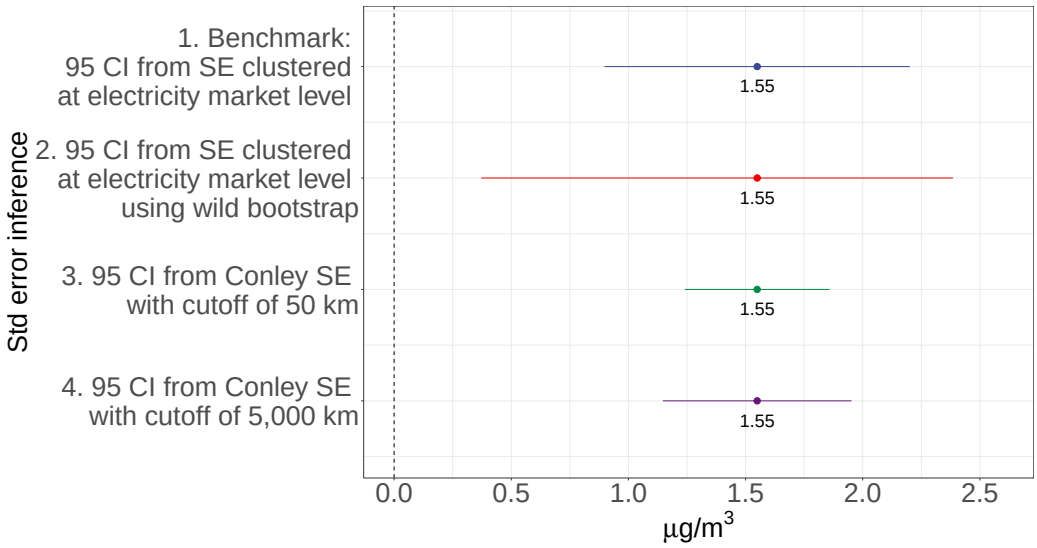

Notes: The figure plots point estimates and 95 percent confidence intervals (CI) of β in Equation 1. All specifications use FHD as our preferred measure of hydrological drought (HD). The CIs are derived from four types of standard errors. Model 1 uses standard errors clustered at the market level. Model 2 uses standard errors clustered at the market level but accounts for few clusters using the wild bootstrap methodology. See MacKinnon and Webb (2017) for details of the calculation. Models 3 and 4 use Conley errors that assume all available lags and the cutoff described in the axis title. See Colella et al. (2019) for details of the calculation.

Figure A5: Effect of FHD on $PM_{2.5}$ concentrations under alternative definitions of drought duration

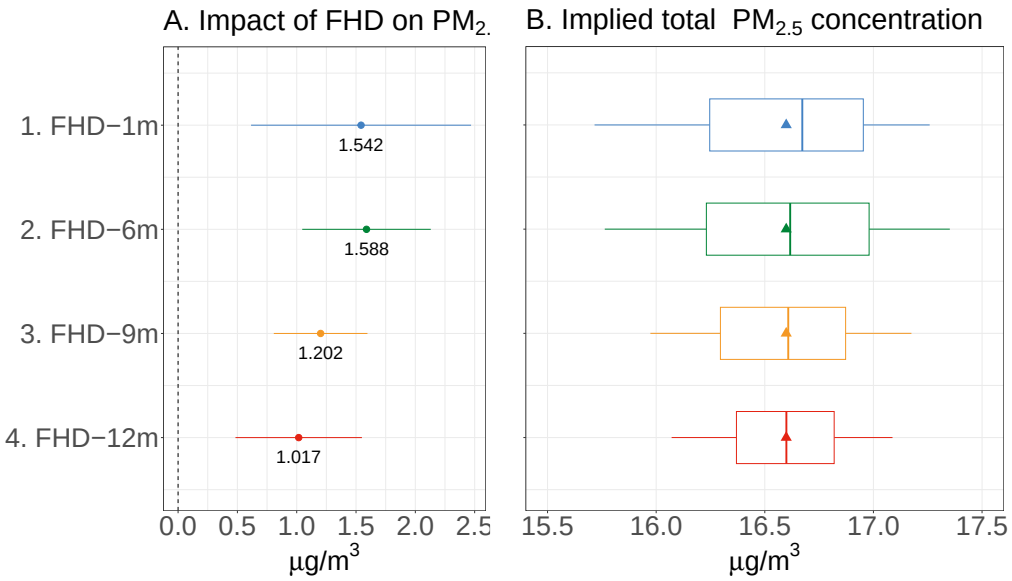

Notes: Panel A plots point estimates and 95 percent confidence intervals (CIs) of β in Equation 1. The CIs are derived from standard errors clustered at the market level. All specifications use FHD as the measure of hydrological drought (HD). Each model uses a version of the FHD derived under the definition of drought listed in the axis title. Panel B plots the distribution of implied total $PM_{2.5}$ concentrations, that is, the marginal effect plus the predicted level of $PM_{2.5}$ in the absence of droughts. The box represents the interquartile range, the whiskers report the minimum and maximum value, and the triangles indicate the average value.

Figure A6: Robustness of estimates under alternative definitions of treatment and outcome

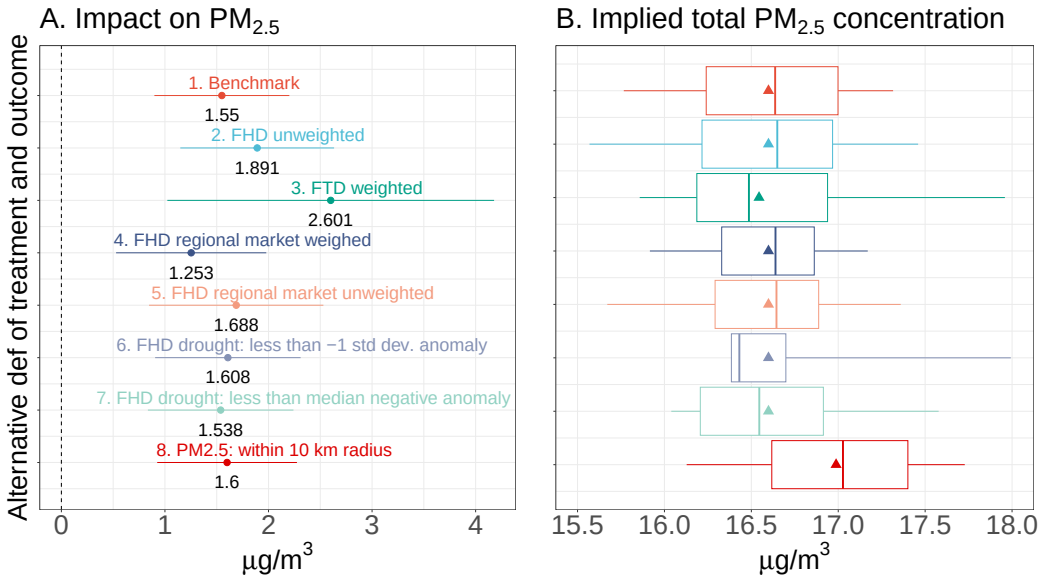

Notes: Panel A plots point estimates and 95 percent confidence intervals (CI) of β in Equation 1. The CIs are derived from standard errors clustered at the market level. Models 1 to 7 report estimates from equation 1, each using the market-level measure of hydropower generation affected by drought listed on top of the coefficient. Model 8 reports estimates from Equation 1 when the outcome is $PM_{2.5}$ concentrations within 10 km of a combustion power plant. Panel B plots the distribution of implied total $PM_{2.5}$ concentrations, that is, the marginal effect plus the predicted level of $PM_{2.5}$ in the absence of droughts. The box represents the interquartile range, the whiskers report the minimum and maximum value, and the triangles indicate the average value.

Figure A7: Robustness of estimates under alternative definitions of the treatment

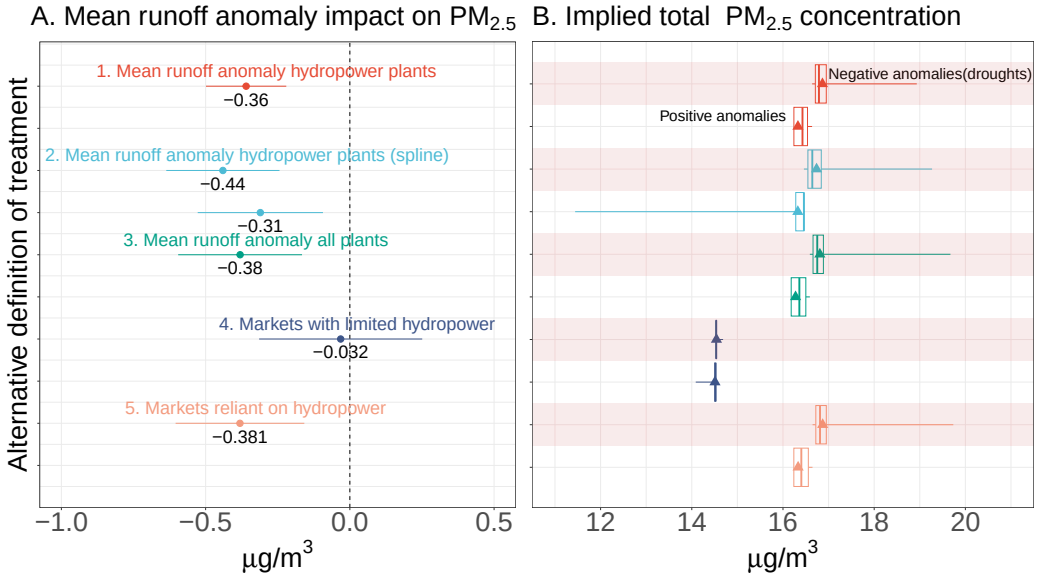

Notes: Panel A plots point estimates and 95 percent confidence intervals (CIs) of β in Equation 1. The CIs are derived from standard errors clustered at the market level. Models 1 to 5 estimate Equation 1, each using the hydrological drought measure listed on top of the coefficient. Negative coefficients imply an increase in pollution for droughts (negative runoff anomalies) and a decrease in pollution for downpours (positive runoff anomalies). Markets with limited hydropower are those with less than 20 percent of the generation coming from hydropower, and markets reliant are those with 20 percent or more. Panel B plots the distribution of implied total $PM_{2.5}$ concentrations, that is, the marginal effect plus the predicted level of $PM_{2.5}$ in the absence of droughts. The box represents the interquartile range, the whiskers report the minimum and maximum value, and the triangles indicate the average value.